

20060921358 -

ADA 131052

Unclassified

SECURITY CLASSIFICATION OF THIS PAGE (When Data Entered)

REPORT DOCUMENTATION PAGE		READ INSTRUCTIONS BEFORE COMPLETING FORM
1. REPORT NUMBER	2. GOVT ACCESSION NO.	3. RECIPIENT'S CATALOG NUMBER
4. TITLE (and Subtitle) TRANSIENT HEAT FLOW ACROSS UNI-DIRECTIONAL FIBERS IN COMPOSITES		5. TYPE OF REPORT & PERIOD COVERED Nov. 1981 - Dec. 1982
7. AUTHOR(s) Lit S. Han Moshen Bashizadeh-Fakhar		6. PERFORMING ORG. REPORT NUMBER 711129
9. PERFORMING ORGANIZATION NAME AND ADDRESS The Ohio State University Research Foundation 1314 Kinnear Road, Columbus, Ohio 43212		8. CONTRACT OR GRANT NUMBER(s) AFOSR-78-3640 F33615-79-C-3030
11. CONTROLLING OFFICE NAME AND ADDRESS Air Force Wright Aeronautical Laboratories Mr. Nelson Wolf, AFWAL/FIBRA		10. PROGRAM ELEMENT, PROJECT, TASK AREA & WORK UNIT NUMBERS
14. MONITORING AGENCY NAME & ADDRESS (if different from Controlling Office)		12. REPORT DATE January 1983
		13. NUMBER OF PAGES
		15. SECURITY CLASS. (of this report) Unclassified
		15a. DECLASSIFICATION/DOWNGRADING SCHEDULE
16. DISTRIBUTION STATEMENT (of this Report) Approved for public release; distribution unlimited		
17. DISTRIBUTION STATEMENT (of the abstract entered in Block 20, if different from Report)		
18. SUPPLEMENTARY NOTES		
19. KEY WORDS (Continue on reverse side if necessary and identify by block number) Transient, heat-flow, composites, fibers, heat penetration		
20. ABSTRACT (Continue on reverse side if necessary and identify by block number) Transient heat flow in fibrous composites is important in determining the depth of heat penetration and temperature gradients near surface layers. A previous report dealt with heat flow parallel to the fiber axis. This research is concerned with heat flow perpendicular to the uni-directional fibers. Temperature responses under the condition of a constant surface heat load are calculated by a finite-difference approach. The rise of the composite surface temperature is governed by two bounding-limits (the effective bound and the matrix bound) de-		

pending on the time scale. A threshold time criterion is established in this research which is based on a heat penetration concept.

... ..

... ..

... ..

... ..

TRANSIENT HEAT FLOW ACROSS
UNI-DIRECTIONAL FIBERS IN COMPOSITES
- A NUMERICAL STUDY -

Lit S. Han¹ and Moshen Bashizadeh-Fakhar²

Department of Mechanical Engineering
The Ohio State University
Columbus, Ohio

January 1983

¹Professor of Mechanical Engineering

²Graduate Research Associate; now instructor, The Ohio State University,
Lima Campus

FOREWORD

This phase of research being a part of a heat transfer study in composites was initiated while an Air Force grant (AFOSR-78-3640) was in effect. The grant by the U.S. Air Force to The Ohio State University Research Foundation was administered and directed by Mr. Nelson Wolf and Lt. S. Kay Bryan of the Air Force Flight Dynamics Laboratory, Wright-Patterson Air Force Base, Dayton, Ohio.

The study in this report was completed in December, 1982, with further support by the Flight Dynamics Laboratory through a contract (F33615-79-C-3030). The support and direction of Mr. Wolf and Lt. Bryan are appreciated by the authors.

TABLE OF CONTENTS

	Page
FOREWORD	iii
LIST OF FIGURES	vii
LIST OF TABLES	ix
NOMENCLATURE	xi
Section	
I. INTRODUCTION	1
II. PROBLEM STATEMENT	5
III. TEMPERATURE RESPONSES	31
III.1 Range of Parametric Variations	31
III.2 Limiting Temperature Distributions - Asymptotic Cases	35
III.2.1 Early-Time Threshold	35
III.2.2 Later-Time Threshold	40
III.3 Surface Temperature Responses	42
III.4 Transverse Distributions of the Composite Surface Temperatures	54
III.5 Temperature Distributions Along the Heat-Flow Direction	59
IV. CONCLUSIONS	77
REFERENCES	81

LIST OF FIGURES

Figure	Page
2.1 Parallel fiber arrays	6
2.2 Layer positions in rectangular array	7
2.3 Single-layer representation of composite	7
2.4 Two-fiber composite	8
2.5 Demonstrative cell and boundary conditions	10
2.6 Node positions in a typical cell	16
2.7 Approximation of the circular interface	18
2.8 Classifications of nodes	20
2.9 Heat balance for type 1 nodes	21
2.10 A nodal point on the insulated end	26
3.1 Configuration for the two-fiber composite under study	32
3.2 Spatial temperature distribution due to a constant heat-flux to a half-space	38
3.3 Average surface temperature rises, Case 1	44
3.4 Average surface temperature rises, Case 2	45
3.5 Average surface temperature rises, Case 3	46
3.6 Average surface temperature rises, Case 6	47
3.7 Average surface temperature rises, Case 7	48
3.8 Average surface temperature rises, Case 8	49
3.9 Average surface temperature rises, Case 9	50

Figure	Page
3.10 Average surface temperature rises, Case 11	51
3.11 Average surface temperature rises, Case 12	52
3.12 Transverse variations of the surface temperatures at $\bar{\theta} = 1$, Case 7	58
3.13 Transverse-average temperature profile in the x-direction at $\bar{\theta} = 0.1$, Case 1	61
3.14 Transverse-average temperature profile in the x-direction at $\bar{\theta} = 0.25$, Case 1	62
3.15 Transverse-average temperature profile in the x-direction at $\bar{\theta} = 0.50$, Case 1	63
3.16 Transverse-average temperature profile in the x-direction at $\bar{\theta} = 4$, Case 1	65
3.17 Transverse-average temperature profile in the x-direction at $\bar{\theta} = 10$, Case 1	66
3.18 Two-dimensional temperature distribution in composite, $\bar{\theta} = 0.5$, Case 1	68
3.19 Two-dimensional temperature distribution in composite, $\bar{\theta} = 5.0$, Case 1	69
3.20 Transverse-average temperature profile in the x-direction at $\bar{\theta} = 0.5$, Case 7	71
3.21 Transverse-average temperature profile in the x-direction at $\bar{\theta} = 5.0$, Case 7	72
3.22 Two-dimensional temperature distribution in composite, $\bar{\theta} = 0.5$, Case 7	74
3.23 Two-dimensional temperature distribution in composite, $\bar{\theta} = 5.0$, Case 7	75
3.24 Transverse-average temperature rise at $\bar{x} = 1.25$, Case 7	76

LIST OF TABLES

Table		Page
3.1	TABULATION OF THERMAL PROPERTIES OF DIFFERENT CASE STUDIES, REFERENCE VALUES: $k_f = 230$, $(\rho c)_f = 51$	36
3.2	CHARACTERISTIC VALUES OF DIFFERENT CASE STUDIES	41

NOMENCLATURE

a	fiber radius
b	half thickness of a layer
\bar{b}	non-dimensional, (b/a)
c	specific heat
d	distance between surface and nearest fiber
\bar{d}	non-dimensional, (d/a)
E	fiber-to-matrix conductivity ratio
H	fiber-to-matrix diffusivity ratio
k	thermal conductivity
L	total length of a composite specimen, see Figure 2.5
M	number of divisions along the x-direction
N	number of divisions along the y-direction
q	heat flow
Q	surface heat flux
T	temperature
\bar{T}	non-dimensional temperature (Tk_f/aQ)
v	volume fraction of total
x	axial coordinate
\bar{x}	non-dimensional, (x/a)
y	transverse coordinate
\bar{y}	non-dimensional, (y/a)

Greek Letters

α	thermal diffusivity, $(k/\rho c)$
$\bar{\lambda}$	$(\Delta \bar{\theta})/(\Delta \bar{x})^2$
θ	time
$\bar{\theta}$	non-dimensional time $(\alpha_f \theta/a^2)$
ρ	density
η	similarity variable

Subscripts

av	refers to the transverse-average value (temperature)
e	refers to effective medium
f	refers to fiber material
i,j	finite-difference direction subscripts (indexes)
m	refers to matrix material
s	refers to surface

SECTION I

INTRODUCTION

With increasing use of composite materials in industries, their applications have been extended to areas where thermal properties are a critical concern. Consequently, thermal responses of composites under operational conditions become important and constitute a significant criterion for their selections in specific applications. In principle, thermal responses can be exactly calculated, provided that the thermal properties of the constituents of the composites and their geometrical patterns of distribution or dispersion are known. In reality, however, there are many obstacles along this path of analysis. In the first place, the calculational efforts would be, practically speaking, prohibitive even if the aforementioned provisions are fulfilled, i.e., the thermo-physical properties and dispersion geometries are known a priori. Second, the thermo-physical properties are not well-defined for existing constituents of the present-day composites. And third, their geometrical patterns of dispersion are only describable in statistical terms. For these reasons, current research efforts are being directed to all three aspects.

To circumvent the enormous expenditure of calculational efforts required in a point-by-point exact analysis of thermal responses in composites, a viable approach is to consider a simplified one-medium bulk

replacing a real composite body; the medium so construed is to have all the macroscopic attributes of its real counterpart. Thus, if a composite body has directional-dependent thermal properties, the one-medium equivalent--often referred to as the effective medium--would be designated as an orthotropic medium having its thermal conductivities different in the three principal directions. In the past decade or so, considerable research emphasis has been devoted to determine the effective thermal conductivities for composites of various types of geometrical dispersions. Some efforts were experimental; and most are analytical based on statistical concepts or on exact heat conduction analysis for simple geometrical patterns.

In performing thermal analyses based on the equivalence principle, i.e., using effective values in an equivalent orthotropic medium, an implicit shortcoming is the fact that the temperature responses thus obtained are only representatives of those in a real composite. Stated differently, the calculated temperatures are the average values over repeating units of the composite in question. To illustrate this differentiation, consider a very simple case of a layer-composite consisting of alternating layers of two different materials in steady-state heat conduction in a direction transverse to the stacking plane of the layers. The actual temperature distribution consists of a series of zigzag straight lines across the entire composite body; the slope of the temperature lines across layers of one material is different from that across layers of the second material. By an effective-medium approach, however, a single straight line now describes the temperature variation across all layers. The real temperature distribution across one repeating unit--two

adjacent layers of two different materials--are two straight lines with two different slopes determined by the respective thermal conductivities of the materials. In some engineering applications results based on the equivalent principle assumption are adequate, such as to determine the heat flow or other overall performance parameters. In other applications, they may be insufficient, such as to determine the thermal stresses which are governed by relative thermal expansions of the layers in contact with each other. In essence, it is the local temperature distributions that dictate local performance parameters. Hence, the approach using an effective medium, while useful in a majority of applications, must be supplemented by suitable criteria so that the local variations on a micro-structural level can be judged.

For heat flow along uni-directional fibers in composite materials, an approximate method of transient analysis [1] has been devised which gives the overall temperature distributions as well as the local deviations. The method of analysis yielded two important parametric combinations governing the accuracy of the analysis: they are the fiber-matrix conductivity ratio and the fiber-matrix thermal capacity ratio. For heat flow perpendicular to uni-directional fibers in composites, however, the situation is more complex. The principal difficulty lies in the fact that each fiber is a self-enclosed boundary in a binding matrix. Analytically, the entire composite body contains an enormous number of doubly-connected regions for which a comprehensive mathematical treatment is impossible. Consequently, in order to account for the local variances in a real composite material, the method of repeating units, which examines the transient heat flow phenomena across a representative section of a composite body,

must be further scrutinized. In this way, any anomaly or unusual feature can be identified.

In this report, microscopic temperature variations near fiber-matrix interface positions are studied. By varying the thermal properties of the two constituents, the fibers and the matrix material, and by means of the finite-difference method, a sufficient number of combinations of the constituents' thermal properties are studied in this phase of research. It is the purpose of such an undertaking to draw simplified modelling conclusions with regard to heat flow across uni-directional fibers in composite materials in general, so that approximate methods of analysis can be developed which can incorporate those features observed in the present work.

SECTION II

PROBLEM STATEMENT

The simplest form of fibrous composite materials is one in which all fibers are parallel to one another and are surrounded by a matrix material. Depending on how fibers are related to one another, their arrangement patterns can be classified into two categories: (1) staggered array, and (2) rectangular array. Cross-section views of these composites are shown in Figure 2.1. In a staggered array, every other layer of composite is shifted linearly by one-half of the fiber pitch; fiber centers form a rectangle in a rectangular array. In a staggered array they form an equilateral triangle.

Central to the method of simplification to a repeating unit is the fact that for most fibrous composites, the physical dimensions of these fibers are indeed very small compared to the dimensions of the structures into which the composite materials are fabricated. When a structural component is exposed to thermal boundary conditions which are in general not one-dimensional, the individual fibers or the geometrically-similar repeating units are essentially under the influence of one-dimensional heat load conditions. In other words, the surface of a composite structure may be subjected to a non-uniform temperature or non-uniform heat flux, but viewed from the dimensional scale of a fiber or a repeating unit consisting of a number of fibers, the boundary surface temperature non-

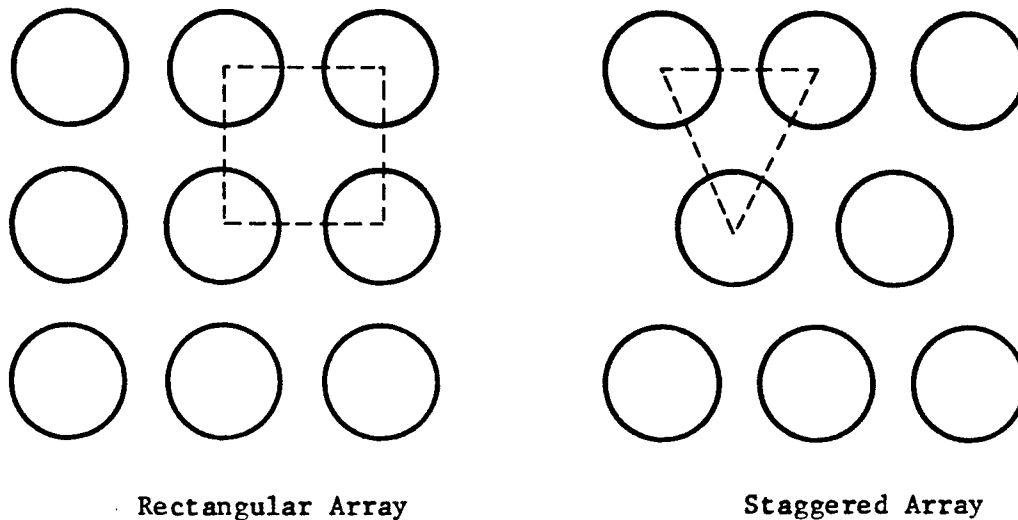


Figure 2.1. Parallel fiber arrays

uniformity or surface heat flux variation becomes negligible from one repeating unit to another. The repeating unit can therefore be considered a one-dimensional problem insofar as the mutual thermal interactions between the fibers and the surrounding matrix materials are concerned.

For heat flow across the uni-directional fibers, a repeating unit is that isolated from a composite body and is shown in Figure 2.2.

Considered in this report is one common type of surface heating: that due to a step-rise of the surface heat flux. By inspecting Figure 2.2, it is evident that when a heat flux is uniformly imparted to the surface, the temperature fields in adjacent layers will be exactly replicates of one another because of geometrical symmetry. Thus, the temperature response of the entire region can be represented by the response of a single layer as shown in Figure 2.3. Also, because the temperature fields in adjacent layers are symmetrical, there is no heat exchange

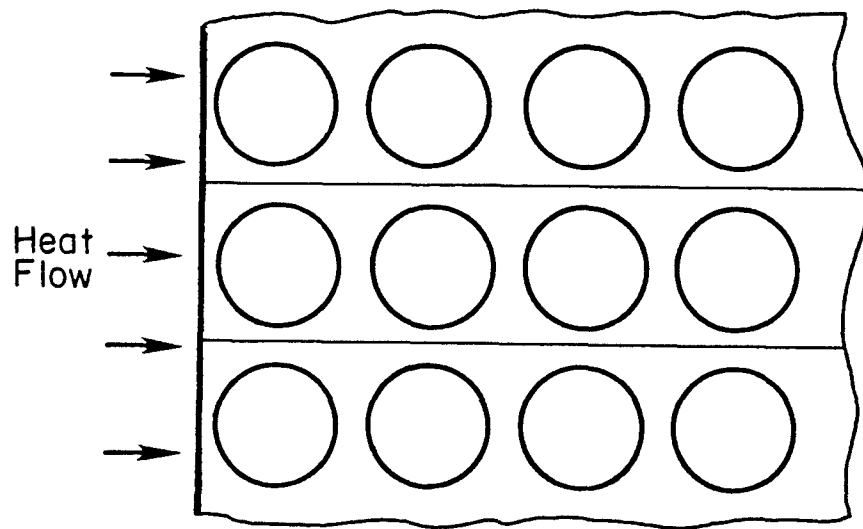


Figure 2.2. Layer positions in rectangular array

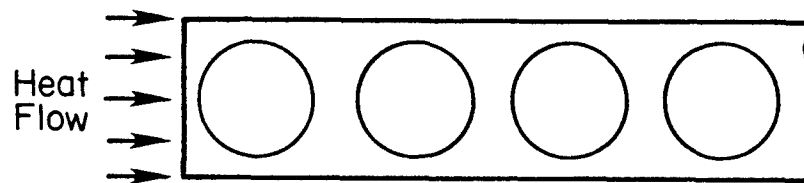


Figure 2.3. Single-layer representation of composite

between individual layers. Thus, the upper and lower boundaries of the reference layer shown in Figure 2.3 are considered as insulated.

Preliminary calculations indicate that when heat is imparted to a composite surface, large temperature differences exist only between the matrix material and the fibers near the surface region at which heat flow originates. And large temperature differences extend to a depth of only one or two fiber diameters. Hence, in order to delineate the micro-structure temperature distribution of the fibers and their surrounding materials, a two-fiber composite configuration as in Figure 2.4 is adopted in this study. The boundary at the end of the two-fiber composite is considered as insulated.

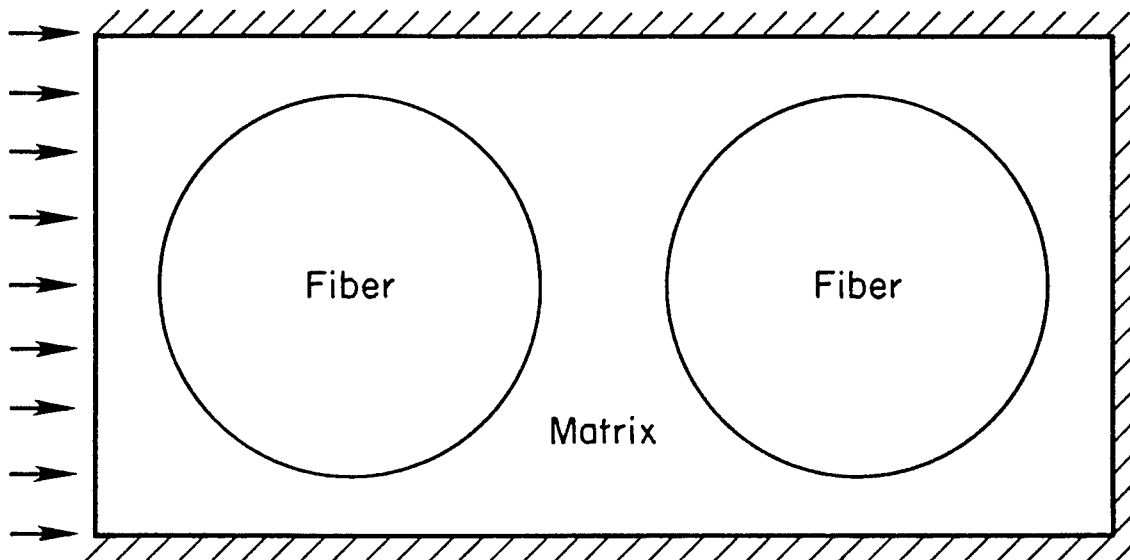


Figure 2.4. Two-fiber composite

With these assumptions, the problem is now reduced to the study of transient heat conduction in a two-fiber composite. Heat flows into the composite in a direction perpendicular to the fiber axis and three sides of the composite are insulated as shown in Figure 2.4.

Next, a finite-difference solution to this problem is formulated.

II.1 THE SOLUTION METHOD

The configuration in Figure 2.4 is the focus of analysis for temperature responses when an impulsive uniform heat flux is imparted to the left surface (non-insulated). Such a configuration represents a prohibitive problem from an analytical viewpoint; a numerical approach is therefore used.

In the numerical approach using a finite-difference method of solving the governing partial differential equations for each region, the entire domain in Figure 2.4 is represented by grid points. The grid points may be arranged either in a rectangular mode or in a circular mode depending on the geometries involved. The former is used in this study.

Insofar as the entire configuration in Figure 2.4 is concerned, there is a repeating pattern from cell to cell, with each cell consisting of a rectangular boundary enclosing a circular fiber in its geometrical center. Hence, in order to show the grid point distribution in the entire configuration, a single cell representation is sufficient. Such a cell is given in Figure 2.5, which outlines the upper half of the unit since the lower half is a mirror image.

For the sake of illustration, the boundary conditions of this demonstrative cell are as indicated, i.e., the insulated boundary condition

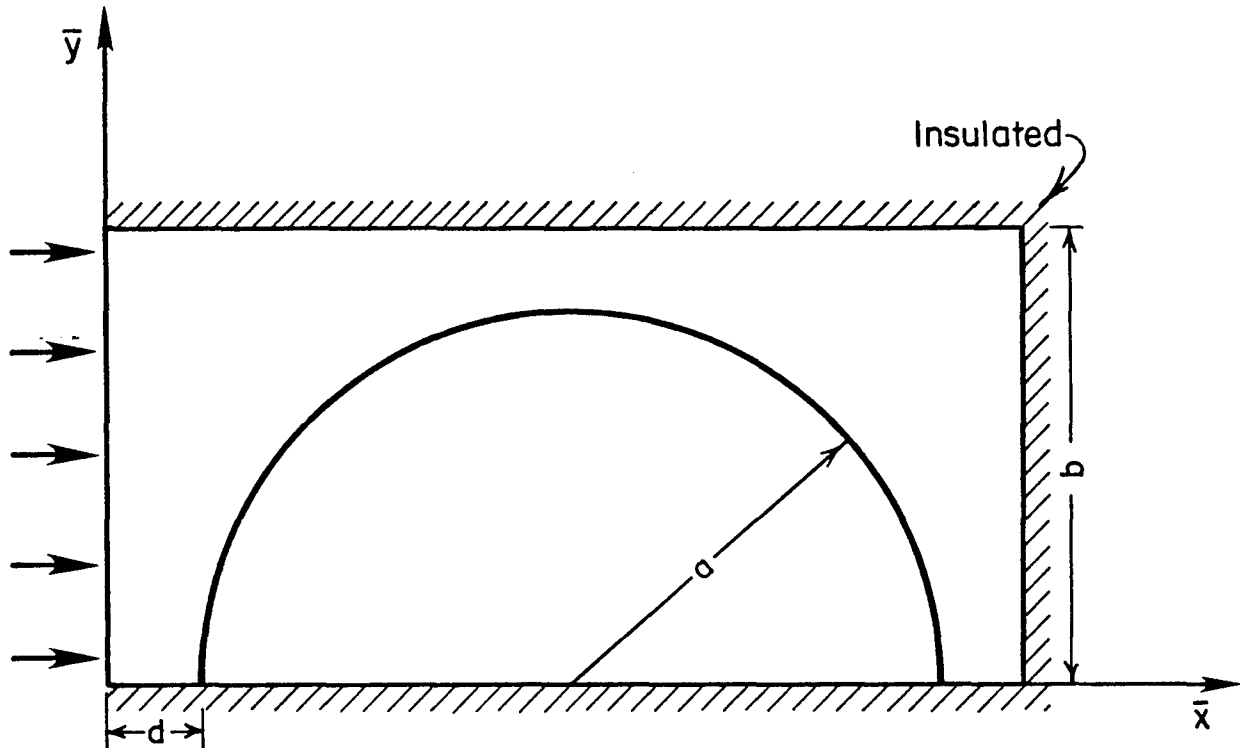


Figure 2.5. Demonstrative cell and boundary conditions

applies at $x = 2(a+d)$, at $y = 0$, and at $y = b$. For a real configuration of more than one cell, the insulated boundary condition at $x = 2(a+d)$ does not apply, but will be transferred downstream to a location $x = 2n(a+d)$ where n indicates the number of cells under consideration.

The employment of only the upper half of a cell for the analysis is justified, since the temperature responses of the two halves will be mirror images of each other. Thus, by making this simplification, the amount of time for numerical calculations will be greatly reduced.

The governing partial differential equation for the thermal response of the fiber and matrix materials is given by the basic diffusion equation. For a two-dimensional heat conduction, the fiber region will be governed by:

$$\partial^2 T_f / \partial x^2 + \partial^2 T_f / \partial y^2 = [(\rho c)_f / k_f] (\partial T_f / \partial \theta) \quad (II.1)$$

and for the regions occupied by the matrix material, the governing equation is:

$$\partial^2 T_m / \partial x^2 + \partial^2 T_m / \partial y^2 = [(\rho c)_m / k_m] (\partial T_m / \partial \theta) \quad (II.2)$$

To solve these equations, specific boundary conditions are needed. The first boundary condition will be that at the borders $y = 0$ and $y = b$ (insulated), thus:

$$\partial T_m(x, b, \theta) / \partial y = 0 \quad (II.3)$$

$$\partial T_m(x, 0, \theta) / \partial y = 0 \quad (II.4-1)$$

$$\partial T_f(x, 0, \theta) / \partial y = 0 \quad (II.4-2)$$

At the interface of fiber and matrix, the heat fluxes must be the same for both materials, i.e.,

$$k_f (\partial T / \partial n)_f = k_m (\partial T / \partial n)_m \quad (II.5)$$

wherein n indicates the direction normal to the interface between the two materials.

Another boundary condition is, of course, the condition at the non-insulated surface $x = 0$. The boundary condition at $x = 0$ will be a constant uniform flux of heat into the composite at this position:

$$-k_m(\partial T_m/\partial x) = Q = \text{Constant in time}, \quad (\text{II.6})$$

where Q denotes the heat flux magnitude. The boundary condition at the insulated end is:

$$k_m(\partial T_m/\partial x) = 0 \quad \text{at } x = 2(a+d) \quad (\text{II.7})$$

For the initial condition, it is assumed that the initial temperature is zero everywhere. The choice of a zero initial temperature is only a matter of convenience.

$$T(x,y,0) = 0 \quad (\text{II.8})$$

Dimensionless equations often simplify an analysis and are more convenient to use. Thus, the partial differential equations and boundary conditions will be written in non-dimensional forms using characteristic values of the fibers as references. The non-dimensional temperature will be defined as,

$$\bar{T} = (k_f T)/(Qa) \quad (\text{II.9})$$

and the dimensions of the region in Figures 2.4 and 2.5 will be non-dimensionalized with respect to fiber radius a . Hence,

$$\bar{x} = x/a, \quad \bar{y} = y/a \quad (\text{II.10})$$

Also define the non-dimensional time as:

$$\bar{\theta} = \alpha_f \theta / a^2 \quad (\text{II.11})$$

Note that all non-dimensional variables carry a bar, while dimensional variables have no bars. This will be the convention throughout the study.

Using the definitions from Equations II.9 through II.11, the partial differential equations and boundary conditions (Equations II.1 through II.8) become, for the fiber material,

$$\partial^2 \bar{T} / \partial \bar{x}^2 + \partial^2 \bar{T} / \partial \bar{y}^2 = \partial \bar{T} / \partial \bar{\theta} \quad (\text{II.1-a})$$

and for the matrix material,

$$\partial^2 \bar{T} / \partial \bar{x}^2 + \partial^2 \bar{T} / \partial \bar{y}^2 = (\alpha_f / \alpha_m) (\partial \bar{T} / \partial \bar{\theta}) \quad (\text{II.2-a})$$

Equations II.3 and II.4 become:

$$\partial \bar{T} / \partial \bar{y} (\bar{x}, \bar{b}, \bar{\theta}) = 0 \quad (\text{II.3-a})$$

$$\partial \bar{T} / \partial \bar{y} (\bar{x}, 0, \bar{\theta}) = 0 \quad (\text{II.4-a})$$

and Equations II.5 through II.8 will be:

$$k_f (\partial \bar{T} / \partial \bar{n})_f = k_m (\partial \bar{T} / \partial \bar{n})_m \quad (\text{II.5-a})$$

$$(\partial \bar{T} / \partial \bar{x}) = -1 \quad (\text{II.6-a})$$

$$k_m (\partial \bar{T} / \partial \bar{x}) = 0 \quad \text{at} \quad \bar{x} = 2(1+\bar{d}) \quad (\text{II.7-a})$$

$$\bar{T}(\bar{x}, \bar{y}, 0) = 0 \quad (\text{II.8-a})$$

In the next section, finite-difference formulas will be derived for determining the temperature responses in fiber-matrix composites.

II.2 THE FINITE-DIFFERENCE SOLUTION OUTLINE

It is necessary to represent the region in this Figure 2.5 by grid points to perform a finite-difference analysis. To further simplify the problem, a square grid configuration will be used.

The length of the cell ($2a + 2d$) and its width b are divided into M and N small increments of equal length $\Delta \bar{x} = \Delta \bar{y}$, respectively. To avoid extra calculations, the number of increments are so chosen that the segments b , d , and a in Figure 2.5 contain integer numbers of increments, i.e., no fractional grids appear in the cell. Thus, minor adjustments of cell dimensions may be required. These adjustments, however, will be very small compared with the overall cell dimensions and will not affect the results.

Although the number of grids for the cell is arbitrary, it is a significant factor in the memory and time required for computations. It is also a determining factor in the accuracy of the results. Naturally, the more the number of grids, the more accurate are the results. On the other hand, the more the number of grids, the larger is the required computation time. Therefore, the number of grids must be chosen so as to

achieve an optimum in accuracy and computation time. A minimum number of four grids is used for the smallest of segments a , d , and $(b-a)$ in Figure 2.5.

At each intersection point of the grids, a node is located at which the temperature is to be calculated. This pattern results in $M+1$ nodes along the x -axis, and $N+1$ nodes along the y -axis. As it can be seen in Figure 2.6, the entire region is divided into small grids by horizontal and vertical lines which are hereby called rows and columns, respectively. The columns and rows are numbered from left to right, and bottom to top, respectively. For convenience, each of these ordinal numbers starts from 1.

The nodes are located at the intersections of columns and rows and are identified by their column and row numbers. Throughout this discussion, index- i represents the column number; and index- j , the row number of any node.

An important issue in the analysis is the treatment of nodes adjacent to fiber-matrix interface (interface nodes). These nodes can be treated in different ways. In an early study on the effective conductivities of uni-directional fiber-composites, Han and Cosner [2] suggested the use of intermediate points on the interface to compute the temperature of these nodes. The temperature of an intermediate point is found by interpolation between the temperatures of their surrounding nodes. The temperature of interface nodes are then found using intermediate point temperatures. This method, although accurate, requires an extra amount of bookkeeping and also requires a long computation time, especially for

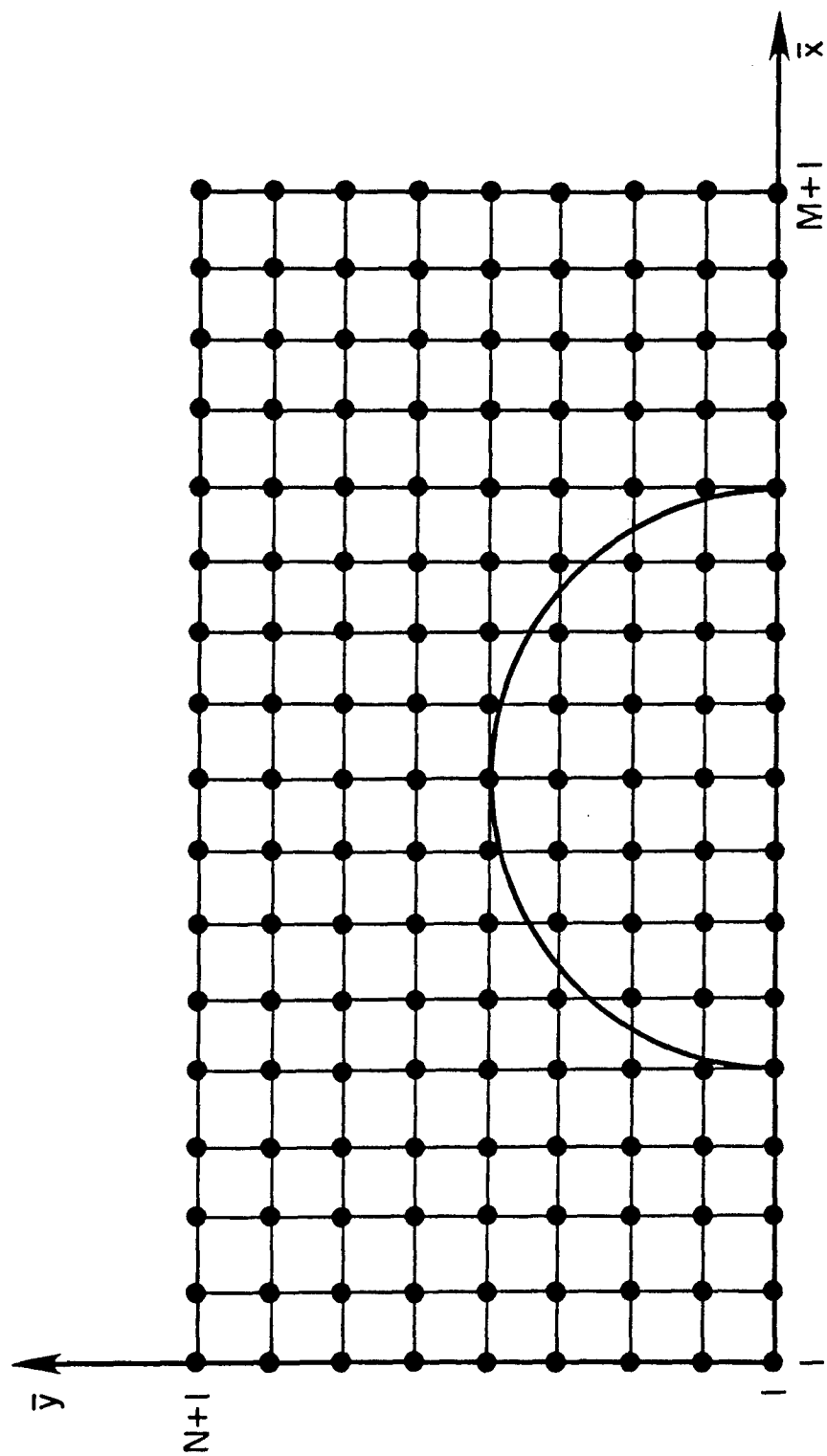


Figure 2.6. Node positions in a typical cell

larger volume ratios and for a composite with more than one cell; therefore, a less complicated method is devised and is described below.

As it can be seen in Figure 2.6, the circular boundary between two regions passes through individual grids (here called interface grids) dividing them into two generally unequal areas. If the number of grids in the cell is large, the area of a grid is small compared to the entire cell area. Also, there will be a large number of interface grids along the circular boundary, and another simplification becomes possible.

If the area of a grid is small, so is the area of a portion of it, that is, the fiber part or matrix part. So, it is not unreasonable to consider the entire interface grid as being either a part of the matrix only or the fiber only, and to ignore the other part while nearly preserving the original volume ratio. This means allocating the entire interface grid to the fiber or to the matrix region depending on which side has a greater portion of the interface grid to begin with. Thus, if the fiber area is larger in the interface grid, that grid will be considered a fiber grid and vice versa. Consequently, the original two-part interface grid is now converted to a one-part grid that belongs to either the fiber region or the matrix region.

Insofar as the shape of the interface boundary is concerned, the circular boundary is now approximated by horizontal and vertical line segments connecting the nodes nearest the interface, and the mathematically exact boundary now follows a zigzag path. The resulting interfacial boundary is presented in Figure 2.7.

The simplification just outlined obviates the calculations for intermediate points, which would be required in other methods. However,

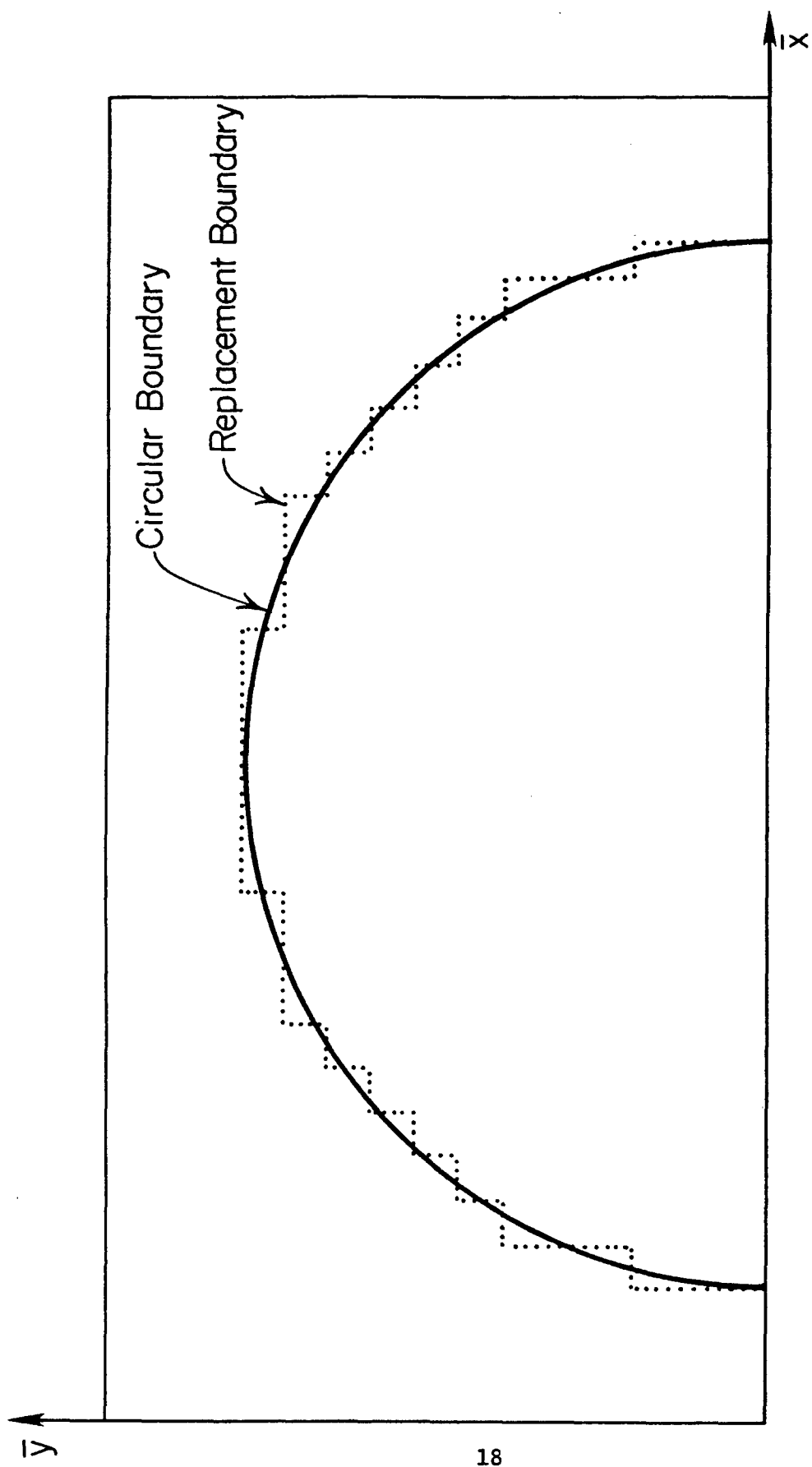


Figure 2.7. Approximation of the circular interface

rearranging the shape of the boundary line results in new "boundary nodes" which require special treatments in the analysis.

By inspecting Figure 2.7, it is seen that it is possible to classify the boundary nodes into seven different types, six of them forming three pairs of mirror images. These types are designated types 1 through 7. The interface nodes are classified according to the positions of their four neighboring nodes. Type 1 nodes are the boundary nodes for which the bottom and top neighboring nodes are also on the interface, while the node on the left belongs to the matrix (matrix node) and the right node is in the fiber (fiber node). Figure 2.8 illustrates this type of nodes.

The fiber and matrix nodes are called types 8 and 9, respectively; these are nodes which are situated respectively in the interior of the fiber and the matrix regions. Shown in Figure 2.8 are also nodes of types 2 through 9. As is apparent in this figure, types 1 and 5 are mirror images of each other, and the other conjugate pairs are types 2 and 6, and types 3 and 7. The shaded areas in this figure indicate the fiber region.

In the next section, finite-difference formulas for the temperature of these nodes are presented.

II.3 THE FINITE DIFFERENCE FORMULAS

Interface and interior nodes. Consider, for example, a node of type 1. The node can be assumed to be at the center of a square grid with a length of $\Delta\bar{x}$ as shown in Figure 2.9. The temperature of the entire grid is represented by the temperature of the node. At a time θ , the temperature of the node is T . To find the temperature of the node at

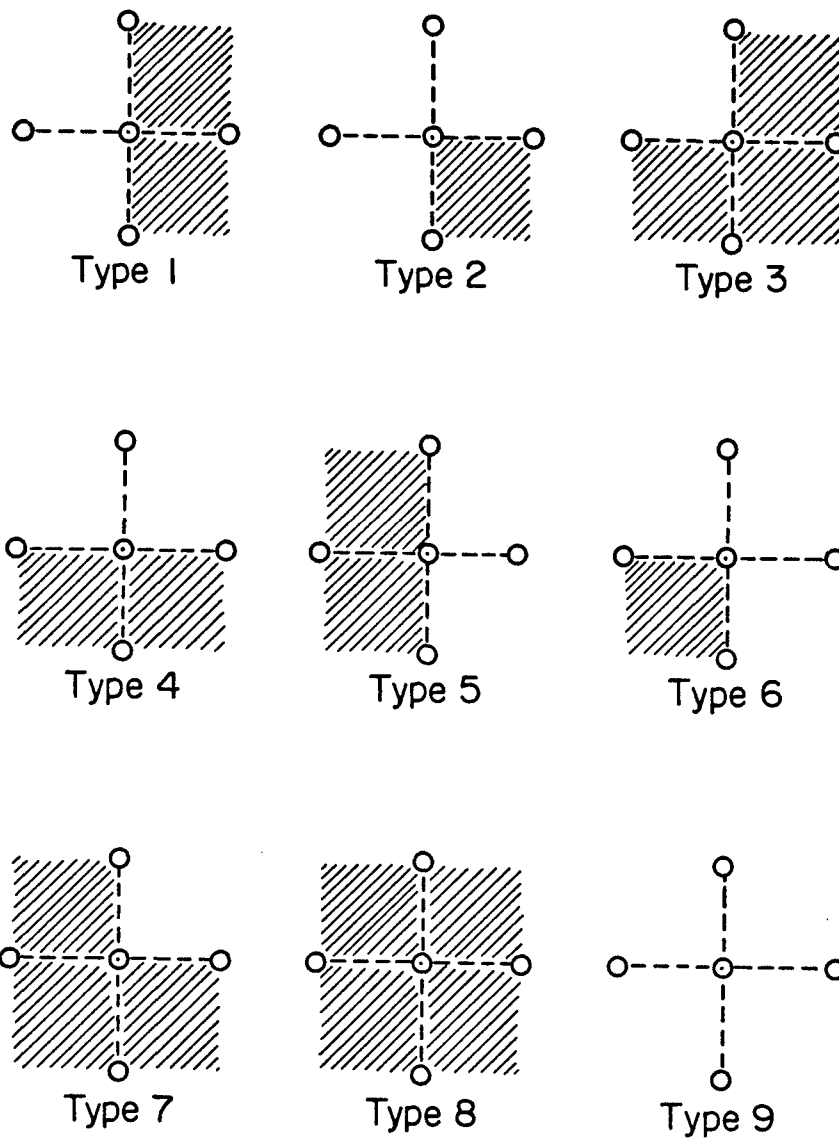


Figure 2.8. Classifications of nodes

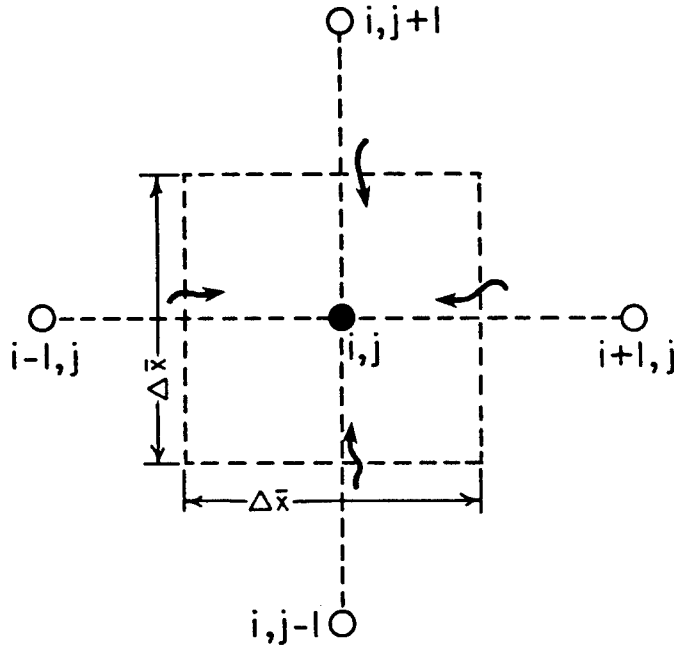


Figure 2.9. Heat balance for type 1 node

a later time, $\theta + \Delta\theta$, an energy balance is written for node (i,j) in Figure 2.9. It should be noted that node $(i-1,j)$ is located in the matrix region and node $(i+1,j)$ is situated in the fiber region. Nodes $(i,j+1)$ and $(i,j-1)$ are also interface nodes.

The heat flux from each of these nodes into (i,j) will be as follows: From $(i-1,j)$ to (i,j)

$$q_{i-1,i} = k_m(T_{i-1,j} - T_{i,j}) \quad (\text{II.12})$$

In Equation II.12, k_m represents the matrix thermal conductivity, and the

index notation $(i-1,i)$ for q indicates that the direction of heat flow is parallel to the rows.

From nodes $(i,j+1)$ and $(i,j-1)$, the heat fluxes into (i,j) consist of two different parts: one through an area of $(\Delta x)/2$ in the matrix region, and the other in the fiber region through an equal area. The heat flows through these two parts are:

$$q_{j-1,j} = (k_f + k_m)(T_{i,j-1} - T_{i,j})/2 \quad (\text{II.13})$$

and

$$q_{j+1,j} = (k_f + k_m)(T_{i,j+1} - T_{i,j})/2 \quad (\text{II.14})$$

where k_f indicates the fiber thermal conductivity.

From node $(i+1,j)$ in the fiber region, the heat flow is:

$$q_{i+1,i} = k_f(T_{i+1,j} - T_{i,j}) \quad (\text{II.15})$$

Counting all the heat fluxes into the central node (i,j) , the total heat input results in a sensible heat change expressed by:

$$\Sigma q = \Sigma mc(\Delta T/\Delta \theta)$$

Here, m indicates mass of each region in the grid (with a depth of unity, of course). Using the non-dimensional variables defined in Equations II.9 and II.10, together with the following:

$$H = \alpha_f / \alpha_m$$

$$E = k_f / k_m$$

A heat balance equation can be used to solve for the future temperature $T'_{i,j}$ in the temperature rise $\Delta T = T'_{i,j} - T_{i,j}$ for the node defined by the indexes i and j . The resulting finite-difference formula for this type of nodes is therefore:

(Type 1)

$$\begin{aligned} \bar{T}'_{i,j} = [\bar{\lambda} / (H+E)] \{ & 2\bar{T}_{i-1,j} + (E+1)\bar{T}_{i,j-1} + 2E\bar{T}_{i+1,j} + (E+1)\bar{T}_{i,j+1} \\ & - [4E + 4 - (H+E) / \bar{\lambda}] \bar{T}_{i,j} \} \end{aligned} \quad (II.16)$$

The same procedure for nodes of Types 2 through 9 results in the following equations.

(Type 2)

$$\begin{aligned} \bar{T}'_{i,j} = [2\bar{\lambda} / (3H+E)] \{ & 2\bar{T}_{i-1,j} + (E+1)\bar{T}_{i,j-1} + (E+1)\bar{T}_{i+1,j} + 2\bar{T}_{i,j+1} \\ & - [6 + 2E - (3H+E) / (2\bar{\lambda})] \bar{T}_{i,j} \} \end{aligned} \quad (II.17)$$

(Type 3)

$$\begin{aligned}\bar{T}'_{i,j} = [2\bar{\lambda}/(H+3E)] \{ & (E+1)\bar{T}_{i-1,j} + 2E\bar{T}_{i,j-1} + 2E\bar{T}_{i+1,j} + (E+1)\bar{T}_{i,j+1} \\ & - [2 + 6E - (H+3E)/(2\bar{\lambda})]\bar{T}_{i,j} \} \end{aligned} \quad (II.18)$$

(Type 4)

$$\begin{aligned}\bar{T}'_{i,j} = [\bar{\lambda}/(H+E)] \{ & (E+1)\bar{T}_{i-1,j} + 2E\bar{T}_{i,j-1} + (E+1)\bar{T}_{i+1,j} + 2\bar{T}_{i,j+1} \\ & - [4 + 4E - (H+E)/\bar{\lambda}]\bar{T}_{i,j} \} \end{aligned} \quad (II.19)$$

(Type 5)

$$\begin{aligned}\bar{T}'_{i,j} = [\bar{\lambda}/(H+E)] \{ & 2E\bar{T}_{i-1,j} + (E+1)\bar{T}_{i,j-1} + 2\bar{T}_{i+1,j} + (E+1)\bar{T}_{i,j+1} \\ & - [4 + 4E - (H+E)/\bar{\lambda}]\bar{T}_{i,j} \} \end{aligned} \quad (II.20)$$

(Type 6)

$$\begin{aligned}\bar{T}'_{i,j} = [2\bar{\lambda}/(3H+E)] \{ & (E+1)\bar{T}_{i-1,j} + (E+1)\bar{T}_{i,j-1} + 2\bar{T}_{i+1,j} + 2\bar{T}_{i,j+1} \\ & - [6 + 2E - (3H+E)/(2\bar{\lambda})]\bar{T}_{i,j} \} \end{aligned} \quad (II.21)$$

(Type 7)

$$\begin{aligned}\bar{T}'_{i,j} = [2\bar{\lambda}/(H+3E)] \{ & 2E\bar{T}_{i-1,j} + 2E\bar{T}_{i,j-1} + (E+1)\bar{T}_{i+1,j} + (E+1)\bar{T}_{i,j+1} \\ & - [2 + 6E - (H+3E)/(2\bar{\lambda})]\bar{T}_{i,j} \} \end{aligned} \quad (II.22)$$

(Type 8) (Fiber Nodes)

$$\bar{T}'_{i,j} = \bar{\lambda}[\bar{T}_{i-1,j} + \bar{T}_{i,j-1} + \bar{T}_{i+1,j} + \bar{T}_{i,j+1} - (4 - 1/\bar{\lambda})\bar{T}_{i,j}] \quad (II.23)$$

(Type 9) (Matrix Nodes)

$$\bar{T}'_{i,j} = (\bar{\lambda}/H)[\bar{T}_{i-1,j} + \bar{T}_{i,j-1} + \bar{T}_{i+1,j} + \bar{T}_{i,j+1} - (4 - H/\bar{\lambda})\bar{T}_{i,j}] \quad (II.24)$$

Boundary nodes. So far, only the interior nodes of the cell have been treated. Now, consider a nodal point on an insulated boundary, as on the insulated end shown in Figure 2.10. The nodal point $(i+1,j)$, which is shown by a dashed-circle in this figure, is the position of a nodal point that would exist on right of (i,j) , had it not been for the insulated boundary.

From a physical point of view, because there is no heat flow from $(i-1,j)$ to $(i+1,j)$, it is concluded that the temperatures of these two nodes

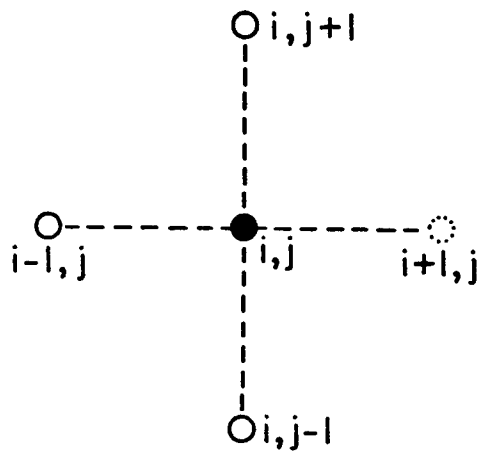


Figure 2.10. A nodal point on the insulated end

must be equal since it is the temperature gradient that causes heat flow. This means that the insulated boundary can be considered as a line of symmetry for the existing temperature field and that an image field of the same geometry exists beyond the insulated boundary.

Thus, node (i,j) can be classified as a regular node (in fiber or matrix) with four neighboring nodes and with $\bar{T}_{i-1,j} = \bar{T}_{i+1,j}$ as a stipulation.

For the configuration in Figure 2.6, the finite different equations for the insulated boundaries can be arrived at from Equations II.23 and II.24, and are shown below.

Bottom Insulated Boundary ($j = 1$)

$$\bar{T}_{i,0} = \bar{T}_{i,2} \quad (\text{see footnote})$$

Fiber Nodes

$$\bar{T}'_{i,1} = \bar{\lambda}[\bar{T}_{i-1,1} + \bar{T}_{i+1,1} + 2\bar{T}_{i,2} - (4 - 1/\bar{\lambda})\bar{T}_{i,1}] \quad (\text{II.25})$$

Matrix Nodes

$$\bar{T}'_{i,1} = (\bar{\lambda}/H)[\bar{T}_{i-1,1} + \bar{T}_{i+1,1} + 2\bar{T}_{i,2} - (4 - H/\bar{\lambda})\bar{T}_{i,1}] \quad (\text{II.26})$$

Top Insulated Boundary ($j = N+1$)

$$\bar{T}_{i,N} = \bar{T}_{i,N+2} \quad (\text{see footnote})$$

$$\bar{T}'_{i,N+1} = (\bar{\lambda}/H)[\bar{T}_{i-1,N+1} + 2\bar{T}_{i,N} + \bar{T}_{i+1,N+1} - (4 - H/\bar{\lambda})\bar{T}_{i,N+1}] \quad (\text{II.27})$$

Insulated End ($i = M+1$)

$$\bar{T}_{M,j} = \bar{T}_{M+2,j} \quad (\text{see footnote})$$

$$\bar{T}_{M+1,j} = (\bar{\lambda}/H)[2\bar{T}_{M,j} + \bar{T}_{M+1,j-1} + \bar{T}_{M+1,j+1} - (4 - H/\bar{\lambda})\bar{T}_{M+1,j}] \quad (\text{II.28})$$

* $\bar{T}_{i,0}$ is a fictitious temperature below the bottom insulated boundary on which the temperature is identified as $\bar{T}_{i,1}$. The mirror image gives this expression. Similarly, $\bar{T}_{i,N+2}$ is the mirror image of the temperature $\bar{T}_{i,N}$; so is $\bar{T}_{M+2,j}$ with respect to $\bar{T}_{M,j}$.

The assumptions made for insulated boundary nodes also apply for the corner nodes $(M+1,1)$ and $(M+1,N+1)$. For the corner node $(M+1,1)$, the following holds:

$$\bar{T}_{M,1} = \bar{T}_{M+2,1}$$

$$\bar{T}_{M+1,2} = \bar{T}_{M+1,0}$$

Thus, for this node:

$$\bar{T}'_{M+1,1} = (\bar{\lambda}/H)[2\bar{T}_{M,1} + 2\bar{T}_{M+1,2} - (4 - H/\bar{\lambda})\bar{T}_{M+1,1}] \quad (\text{II.29})$$

For the top corner node $(M+1,N+1)$, the finite-difference formulas are:

$$\bar{T}_{M,N+1} = \bar{T}_{M+2,N+1}$$

$$\bar{T}_{M+1,N} = \bar{T}_{M+1,N+2}$$

then:

$$\bar{T}'_{M+1,N+1} = (\bar{\lambda}/H)[2\bar{T}_{M,N+1} + 2\bar{T}_{M+1,N} - (4 - H/\bar{\lambda})\bar{T}_{M+1,N+1}] \quad (\text{II.30})$$

Having the finite-difference equations for all nodes in the cell, a computer program can be formulated to find the future temperatures of all nodes.

II.4 THE STABILITY CRITERION

The finite-difference equations shown in Section II.3 for different nodes in the composite cell are not always convergent; that is, they do not always tend to the solution of the partial differential equation, as grid and time spacings tend to zero. Therefore, certain conditions must be met to assure convergence and to achieve the best approximate solutions. This condition is known as the stability criterion.

For a fixed grid size, there is an upper limit for $\Delta\theta$ beyond which some errors will occur in calculations (beside round-off errors), and these errors will be amplified as computations continue until the results become meaningless. To prevent this from occurring, a stability criterion must be met.

The following example shows how to establish the stability criterion. Consider Equation II.23 and write it as:

$$\bar{T}'_{i,j} = \bar{\lambda}[\bar{T}_{i-1,j} + \bar{T}_{i,j-1} + \bar{T}_{i+1,j} + \bar{T}_{i,j+1}] + [1 - 4\bar{\lambda}]\bar{T}_{i,j}$$

The first set of brackets on the right side of this equation is positive, therefore the second set must also be positive in order to prevent unstable fluctuations. Thus:

$$\bar{\lambda} \leq 1/4 \tag{II.31}$$

Using the definition for $\bar{\lambda}$ in the inequality of Equation II.31 results in:

$$\Delta\theta \leq .25(\Delta x)^2$$

Writing in dimensional form,

$$\alpha_f(\Delta\theta)/(a)^2 \leq .25(\Delta x)^2/(a)^2$$

then:

$$\Delta\theta \leq .25(\Delta x)^2/\alpha_f$$

Therefore, to have stable conditions, the time increment must satisfy the above inequality. For other nodes, also, the time increment must be found in the same fashion. Obviously, the smaller of all time increments must be used in the computer program to satisfy the stability criterion.

SECTION III

TEMPERATURE RESPONSES

III.1 RANGES OF PARAMETRIC VARIATIONS

In order to investigate the thermal responses of fiber composites, a two-fiber composite body as shown in Figure 3.1 is taken and its temperature response when a constant flow of heat is imparted to its surface at $\bar{x} = 0$ is studied. The volume ratio is always taken to be 0.5, representative of the current practice. As it is a typical value for carbon/epoxy composites used in aircraft structures, this ratio together with the assumption that the fibers are arranged in a square pattern results in the dimensions shown in Figure 3.1, in which the fiber radius is taken to be unity. The properties of the fibers considered in this report are arbitrarily taken as follows: $k_f = 230$ and $(\rho c)_f = 51$, both in a consistent set of units. The numerical values of these two parameters are unimportant because it is the relative magnitudes between the values of the two constituents - fiber and matrix - that really govern the heat flow paths and penetration depths, etc. The values taken are therefore a matter of convenience, as shall be seen later.

Following the concept just discussed, the values of $k_f = 230$ and $(\rho c)_f = 51$ are therefore kept constant throughout this study, while the corresponding values for the matrix material are varied such that the ratios between the thermal conductivities and between the thermal capacities

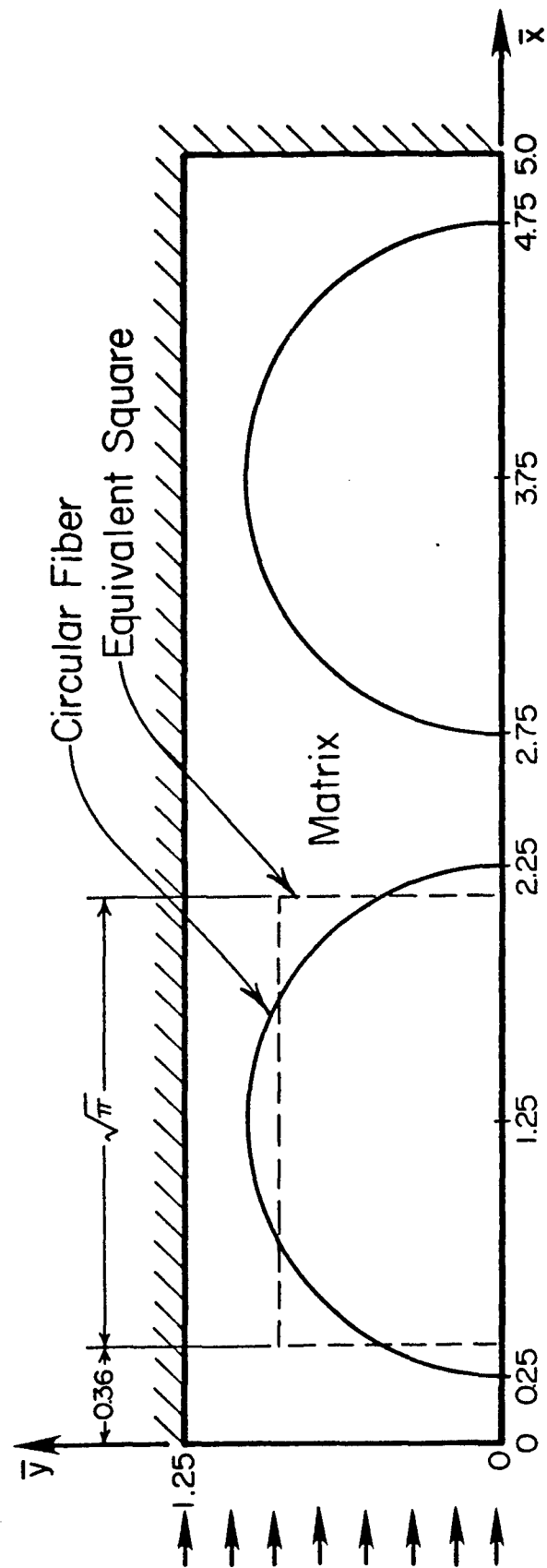


Figure 3.1. Configuration for the two-fiber composite under study

of the two constituents cover a range wide enough to draw meaningful conclusions.

Convenient criteria for judging thermal characteristics of a composite in reference to the basic component materials are the effective values. Two principal ones are: (i) effective thermal conductivity k_e and (ii) effective thermal diffusivity α_e . Effective thermal diffusivities have been studied extensively in the literature and are properties pertaining to unsteady-state conduction phenomena. There are many ways of estimating the effective conductivities which are, however, predicated on a knowledge of the ratio of the constituents' thermal conductivities. In this report, it is clear that it is the ratio of thermal conductivities k_f/k_m that counts, not the numerical value of either one.

The effective thermal diffusivities are conceptually useful for transient conduction analyses in composites when the time scale and the distance scale are such that the temperature variation within one fiber or across one lamination is small compared to the overall temperature changes in the composite body. In other words, a composite medium is now replaced by a homogeneous medium which has property values of k_e and α_e . The temperature responses calculated on that basis would be the same as in the composite medium if a scale larger than that of a fiber is considered as representative. In most fiber-matrix composites, the fiber dimension (radius) is invariably much smaller than the body dimensions (thickness). Hence, the condition on the scale ratio is fulfilled. However, it is the micro-structure temperature changes in the interstices that eventually make up macroscopic temperature changes which are describable by the effective properties k_e and α_e .

In the make-up of the effective thermal diffusivity parameters defined by,

$$\alpha_e = k_e / (\rho c)_e$$

the divisor $(\rho c)_e$ is the effective thermal inertia, and, being a scalar quantity can be obtained simply on a pro rata basis. Hence, the effective value $(\rho c)_e$ can be expressed by the following combination:

$$(\rho c)_e = (\rho c)_f v_f + (\rho c)_m v_m \quad (\text{III.1})$$

where v_f and v_m are the volume fractions of the constituents - fiber and matrix - respectively.

All together, twelve cases were investigated. Values of the physical properties for the matrix medium were chosen in reference to those arbitrarily fixed for the fiber material such that there were four ratios of the effective to matrix conductivities. These are $k_e/k_m = 0.6, 1, 2$ and 3. The first one is obviously the result of fibers being less conductive than the matrix such as carbon fibers in a metal matrix. Conversely, the last value of 3 is the result of fibers being more conductive than the matrix such as carbon fibers in a resin matrix.

With regard to the range of $(\rho c)_e/(\rho c)_m$, four values were intended, namely 0.6, 1.0, 5 and 10. The lower value implies that the fiber medium has a smaller thermal inertia than the matrix medium; and of course, the opposite is true for larger values of 5 and 10. In performing the necessary computations, however, computer time for the last two capacity ratios

$(\rho c)_e/(\rho c)_m$ was found excessive when combined with the first two values of k_e/k_m and it became expedient to restrict the variations of $(\rho c)_e/(\rho c)_m$ to 0.6 and 1.0 only for $k_e/k_m = 0.6$ and 1. Based on Equation III.1, the value of $(\rho c)_m$ can be determined. To specifically determine the matrix conductivity required to yield a desired effective thermal conductivity, the information in Reference [2] was used. With the above described procedure, the cases considered are tabulated in Table 3.1.

In obtaining results for these cases by a finite-difference method, the number of nodes along \bar{x} and \bar{y} axes (referring to Figure 3.1) were kept unchanged for all cases. This is to provide a basis for comparing the results more easily. The computer program calculates non-dimensional temperatures of all nodes for various non-dimensional times. Time was varied up to 10 for all cases except for cases number 2 and 8 in Table 3.1; for these two cases time was varied up to 8 only, because of excessive computer time requirements. Computed results are presented in graphical forms. Several comparisons are also made between the fiber-composite and the corresponding effective medium temperature responses to evaluate the validity of the effective medium approach used for approximating the temperature responses of fiber-composites.

III.2 LIMITING TEMPERATURE DISTRIBUTIONS - ASYMPTOTIC CASES

III.2.1 Early-Time Threshold

In order to synthesize the calculated temperature responses of composites with various thermo-physical properties for fibers and the matrix materials, it is imperative to establish some asymptotic criteria against which the calculated temperatures can be compared. With the configuration

TABLE 3.1

TABULATION OF THERMAL PROPERTIES OF DIFFERENT CASE STUDIES, REFERENCE VALUES: $k_f = 230$,
 $(\rho c)_f = 51$

Case No.	$\frac{k_e}{k_m}$	$\frac{(\rho c)_e}{(\rho c)_m}$	k_m	$(\rho c)_m$	α_m	k_e	$(\rho c)_e$	α_e	$\frac{\alpha_e}{\alpha_m}$	$\frac{\alpha_f}{\alpha_m}$
1	0.6	0.6	680	249.1	0.366	408	149.5	2.73	1.0	1.65
2	0.6	1.0	680	51.	13.3	408	51	8.0	0.6	0.34
3	1.0	0.6	230	249.1	0.923	230	149.5	1.54	1.66	4.88
4	1.0	1.0	230	51	4.51	230	51	4.51	1.0	1.0
5	2.0	0.6	46	249.1	0.185	92	149.5	0.616	3.3	24.42
6	2.0	1.0	46	51	0.902	92	51	1.8	2.0	5.0
7	2.0	5.0	46	5.7	8.07	92	28.5	3.23	0.4	0.56
8	2.0	10.	46	2.7	17.0	92	27.	3.41	0.2	0.265
9	3.0	0.6	2.7	249.1	0.011	8.1	149.5	0.054	5.0	416.
10	3.0	1.0	2.7	5.1	0.053	8.1	51	0.159	3.0	85.2
11	3.0	5.0	2.7	5.7	0.474	8.1	28.5	0.284	0.6	9.52
12	3.0	10.	2.7	2.7	1.0	8.1	27.	0.30	0.3	4.51

defined in Figure 3.1, it is apparent that when heating of the composite starts, the first layer of the material medium encountered is that of the matrix material. Hence during the early stage of a heating period, the temperature distribution in the composite body must be nearly the same as when the fibers are absent. Based on this concept, an early asymptotic solution can be established which is obviously the case of constant surface heat flux to a semi-infinite body consisting entirely of the matrix material. It is well known that such a heating problem is described by the solution:

$$T_m = 2(Q/k_m) \sqrt{\alpha_m \theta} \operatorname{ierfc}(\eta_m) \quad (\text{III.2})$$

where η_m is the similarity variable defined by,

$$\eta_m = x/(2\sqrt{\alpha_m \theta}) \quad (\text{III.3})$$

The spatial temperature distribution is embedded in the error function in Equation (III.2) through the similarity variable and is graphically shown in Figure 3.2. The spatial distribution is given by the curve, which for simplicity's sake can be approximated by two straight-line segments, AB and BC. Line AB is the tangent to the curve at point A and intersects the abscissa at B where $\eta_m = 1/\sqrt{\pi}$. In the simplified picture, heating of a semi-infinite solid is divided into two parts, consisting of a surface layer from $\eta_m = 0$ to $\eta_m = 1/\sqrt{\pi}$, i.e., from A to B and, beyond this surface layer, the remainder of the region in which the temperature remains unaffected.

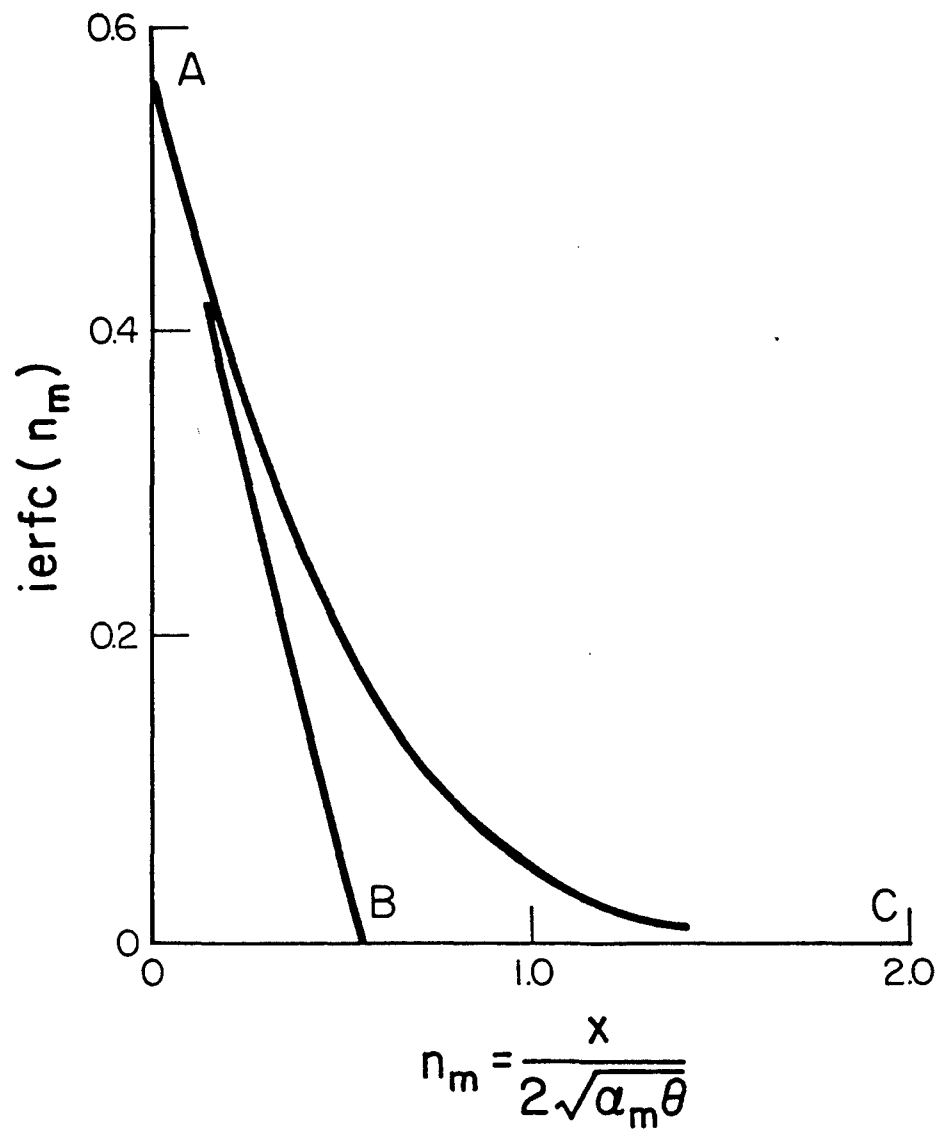


Figure 3.2. Spatial temperature distribution due to a constant heat flux to a half-space.

To relate the preceding discussion to the asymptotic analysis for heat conduction in the fiber-matrix composite defined in Figure 3.1, an average surface layer consisting of the matrix material alone is first established. The reason for the average is that the fibers, being cylindrical in shape, has its forward-most position at $(x/a) = 0.25$ and its largest cross-sectional obstruction at $(x/a) = 1.25$, where the center of the first fiber lies. Replacing the cylindrical fiber by a square fiber with the same area, the resulting equivalent square fiber has, therefore, sides of $\sqrt{\pi}$ in terms of the fiber radius a . The replacement equivalent is devised just for the purpose of establishing an average heat front and is superposed in Figure 3.1 where the frontal surface is located at a distance of $(0.36a)$ from the heating surface. This value represents, of course, an average value taking into consideration the roundedness of the fiber. From such a simplification, it can be stated that before the heat front reaches a position of $x = 0.36a$, heat conduction in the composite body is not different from that in a semi-infinite body of the matrix material alone. Setting η_m to $1/\sqrt{\pi}$, and substituting x by $0.36a$ there results a threshold time, or the early limiting time, θ_{t-1} , given by

$$(\alpha_m \theta_{t-1} / a^2) = (0.36^2 \pi / 4) \quad (\text{III.4})$$

Since in the computational scheme in this study, use is made of a dimensionless time $\bar{\theta} = \alpha_f \theta / a^2$, Equation (III.4) can be expressed by

$$\bar{\theta}_{t-1} = (\alpha_f \theta_{t-1} / a^2) = 0.1(\alpha_f / \alpha_m) \quad (\text{III.5})$$

The significance of the early threshold time is that for time less than that expressed by Equation (III.5). The temperature distribution in the composite is virtually identical to that of a semi-infinite body of the matrix material only. This applied to the depth direction and to the transverse direction as well. Stated in other words, at very small times, the transverse temperature variation, especially on the heating surface, is quite small compared to the average temperature rise. This conclusion is directly opposite to the deduction made in [1] for heat flow parallel to the fiber orientation. For the twelve cases of the physical-property combinations shown in Table 3.1, the early threshold times given by Equation III.5 are listed in Table 3.2 together with the later threshold times to be discussed next.

III.3.2 Later-Time Threshold

As the heating process continues, the matrix material and the fibers are raised to higher temperature levels while conduction into the composite interior proceeds. Under this condition, the entire composite body would behave almost like a single-phase body or a single effective medium. For this event to occur, the depth of heat penetration must include at least one fiber in the interior from the heating surface. To arrive at a quantitative criterion, an effective medium occupying a semi-infinite space is used; the temperature response due to heating of the surface is analogous to Equations III.2 and III.3, except the physical properties are now those of the effective medium. The heating depth is obtained from Figure 3.1 at the rear of the square-equivalent, i.e., $x = (0.36 + \sqrt{\pi})a$. Setting $\eta_e = 1/\sqrt{\pi}$ and using the similarity variable

TABLE 3.2
CHARACTERISTIC VALUES OF DIFFERENT CASE STUDIES

CASE NO.	EARLY-TIME THRESHOLD, $\bar{\theta}_{t-1}$ (Equation III.5)	LATER-TIME THRESHOLD, $\bar{\theta}_{t-2}$ (Equation III.7)	$1/\sqrt{k_m(\rho c)_m}$ (Note 2)	$1/\sqrt{k_e(\rho c)_e}$ (Note 2)
1	0.165	5.91	0.243×10^{-2}	0.404×10^{-2}
2	0.034	2.04	0.54×10^{-2}	0.698×10^{-2}
3	0.488	10.5	0.417×10^{-2}	0.539×10^{-2}
4	0.1	3.56	0.921×10^{-2}	0.921×10^{-2}
Note 1 5	2.44	26.5	0.932×10^{-2}	0.848×10^{-2}
Note 1 6	0.5	9.0	2.07×10^{-2}	1.45×10^{-2}
7	0.056	5.0	6.16×10^{-2}	1.95×10^{-2}
8	0.0265	4.8	8.90×10^{-2}	2.0×10^{-2}
9	41.6	298	3.87×10^{-2}	2.83×10^{-2}
10	8.52	102	8.48×10^{-2}	4.90×10^{-2}
11	0.95	56.9	25.3×10^{-2}	6.60×10^{-2}
12	0.451	53.7	37.0×10^{-2}	6.70×10^{-2}

¹Reference Case $(\rho c)_m = (\rho c)_f = (\rho c)_e$, $k_m = k_f = k_e$

²Based on reference values for fibers: $k_f = 51$, $(\rho c)_f = 231$

η_e as defined by Equation III.3 for η_m , the later threshold time can be expressed as:

$$(\alpha_e \theta_{t-2}/a^2) = (0.36 + \sqrt{\pi})^2 \pi/4 = 3.56 \quad (\text{III.6})$$

Using the non-dimensional time $\bar{\theta}$, Equation III.6 is recast as

$$\bar{\theta}_{t-2} = (\alpha_f \theta_{t-2}/a^2) = 3.56(\alpha_f/\alpha_e) \quad (\text{III.7})$$

and for the twelve cases investigated, the later threshold times are listed in Table 3.2.

III.3 SURFACE TEMPERATURE RESPONSE - TRANSVERSE-AVERAGE VALUE

One of the most important performance parameters is the surface temperature variation of the composite when a heat flux is imparted onto the surface. Since the first layer encountered by the oncoming heat flux is the matrix material, the surface temperature response of a semi-infinite body comprised of the matrix material only must constitute one of the two temperature bounds for a real composite body. And as time proceeds, the effect of fibers embedded in the composite are brought into play; consequently, the surface temperature variation at the later stage of the process will be nearly the response by a single-phase medium whose physical properties are the effective values. The surface temperature variation based on the effective-medium calculation is then the other limiting envelope. The computed surface temperature rise of a real composite, therefore, lies between these two limits which are expressed by:

$$T_{e-s} = (2Q\sqrt{\theta/\pi}) / \sqrt{k_e(\rho c)_e} \quad (\text{III.8})$$

$$T_{m-s} = (2Q\sqrt{\theta/\pi}) / \sqrt{k_m(\rho c)_m} \quad (\text{III.9})$$

These two expressions for the surface temperature responses are derived from Equation (III.2) by setting $\eta_m = 0$ and show the well-known phenomenon that the surface temperature rise is inversely proportional to the quantity $\sqrt{(k\rho c)}$ of a single-phase medium. The numerical values of $\sqrt{(k\rho c)}$ based on the effective-medium values and the matrix-medium values for the twelve cases investigated are listed in Table 3.2. Note that the tabulation is based on arbitrary set of k_f , $(\rho c)_f$, i.e., $k_f = 231$ and $(\rho c)_f = 51$.

A merit of the tabulation in Table 3.2 is that the limiting temperature rises, being proportional to the values in the last two columns, can be discerned immediately. As an example, Case 2 lists the values of 0.17×10^{-2} and 0.693×10^{-2} in the last two columns, indicating that the temperature rise based on the effective-medium calculation is four times as large as that calculated on the basis of the matrix material alone. For case No. 8, the opposite is true. The transversely averaged surface temperature for all cases rises with time, but is bracketed by these two limiting bounds - referred to, hereafter, as the matrix-bound and effective-bound, respectively. For all twelve cases of the physical-property combinations listed in Table 3.1, their transversely averaged surface temperatures are displayed in Figures 3.3 through 3.11; for cases 4, 5, and 9, their variations are not presented because of the following reasons. Case 5 shows that the physical-property combinations give the matrix-bound

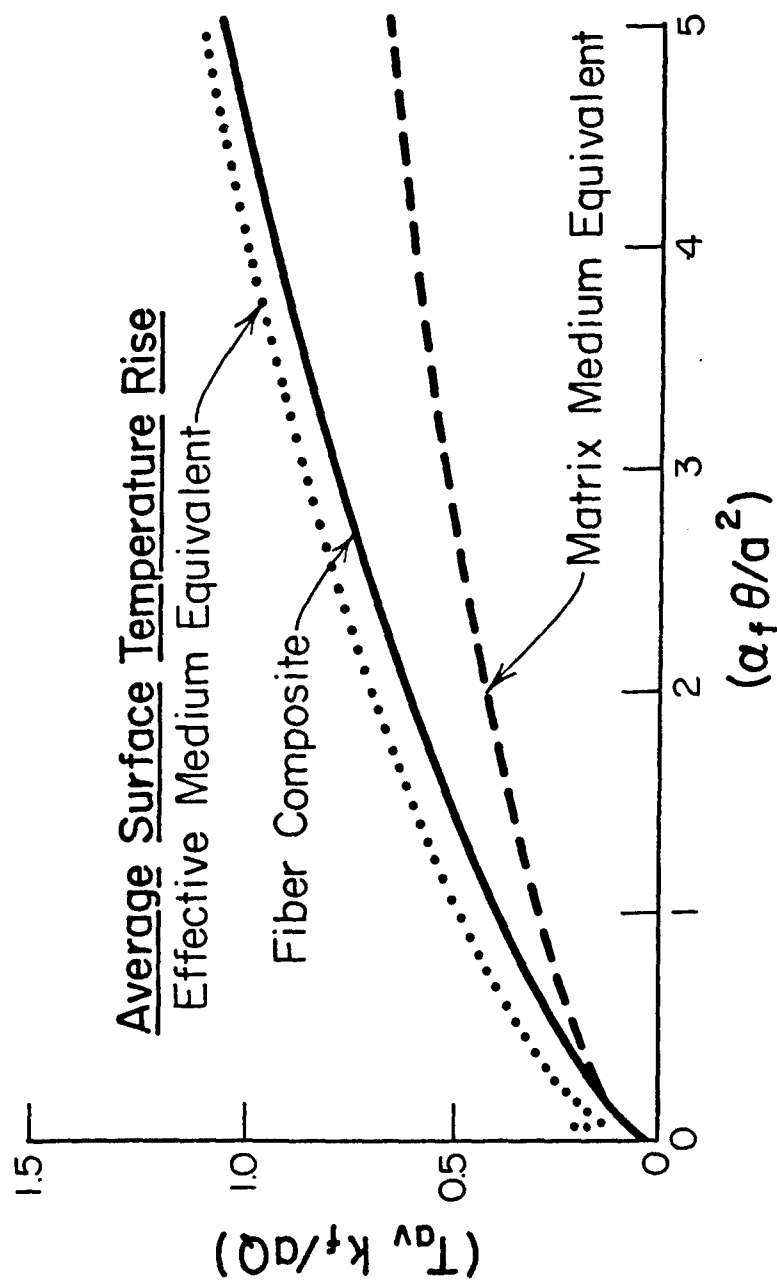


Figure 3.3. Average surface temperature rises, Case 1

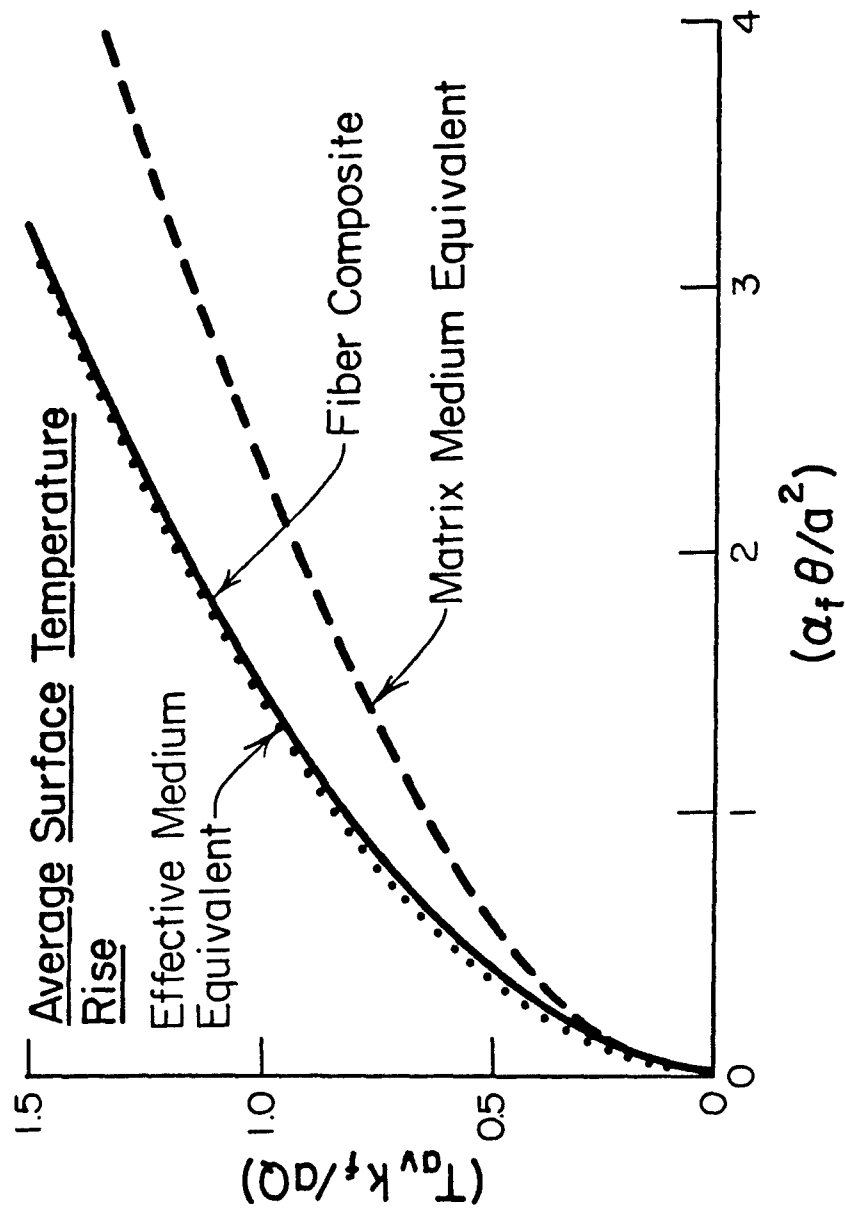


Figure 3.4. Average surface temperature rises, Case 2

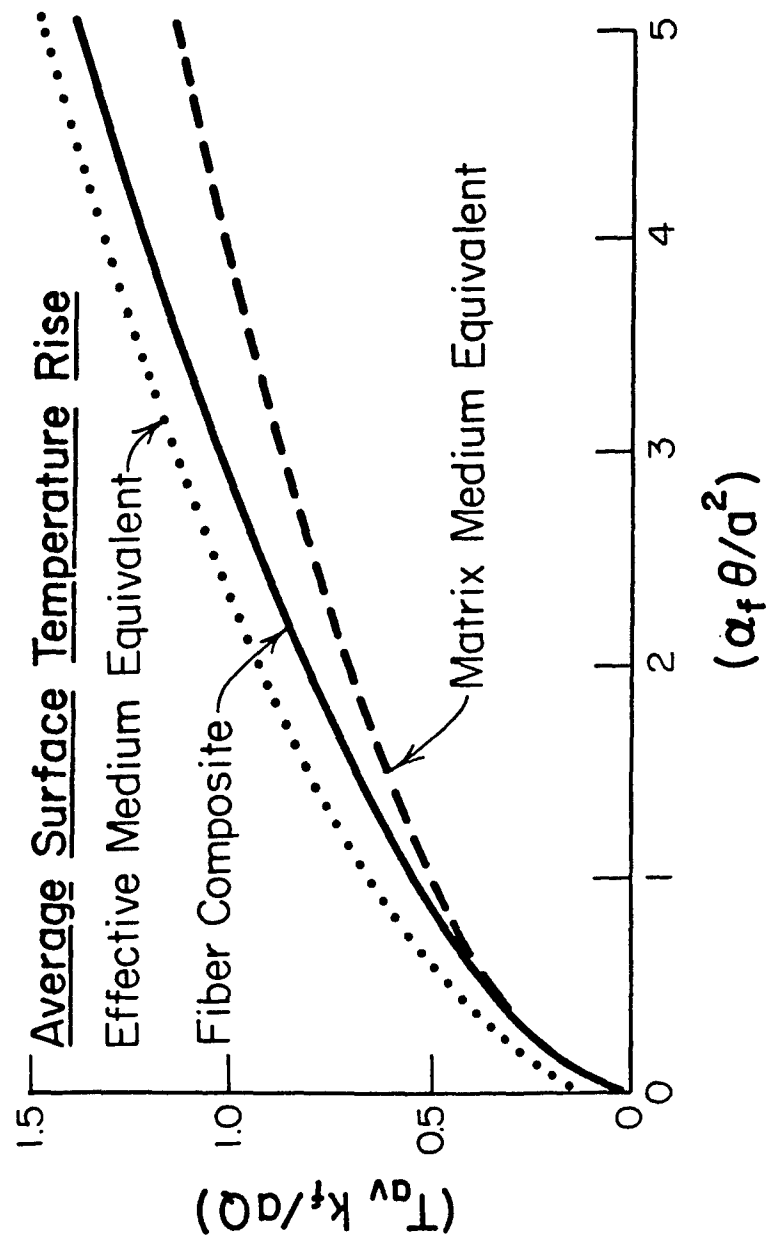


Figure 3.5. Average surface temperature rises, Case 3

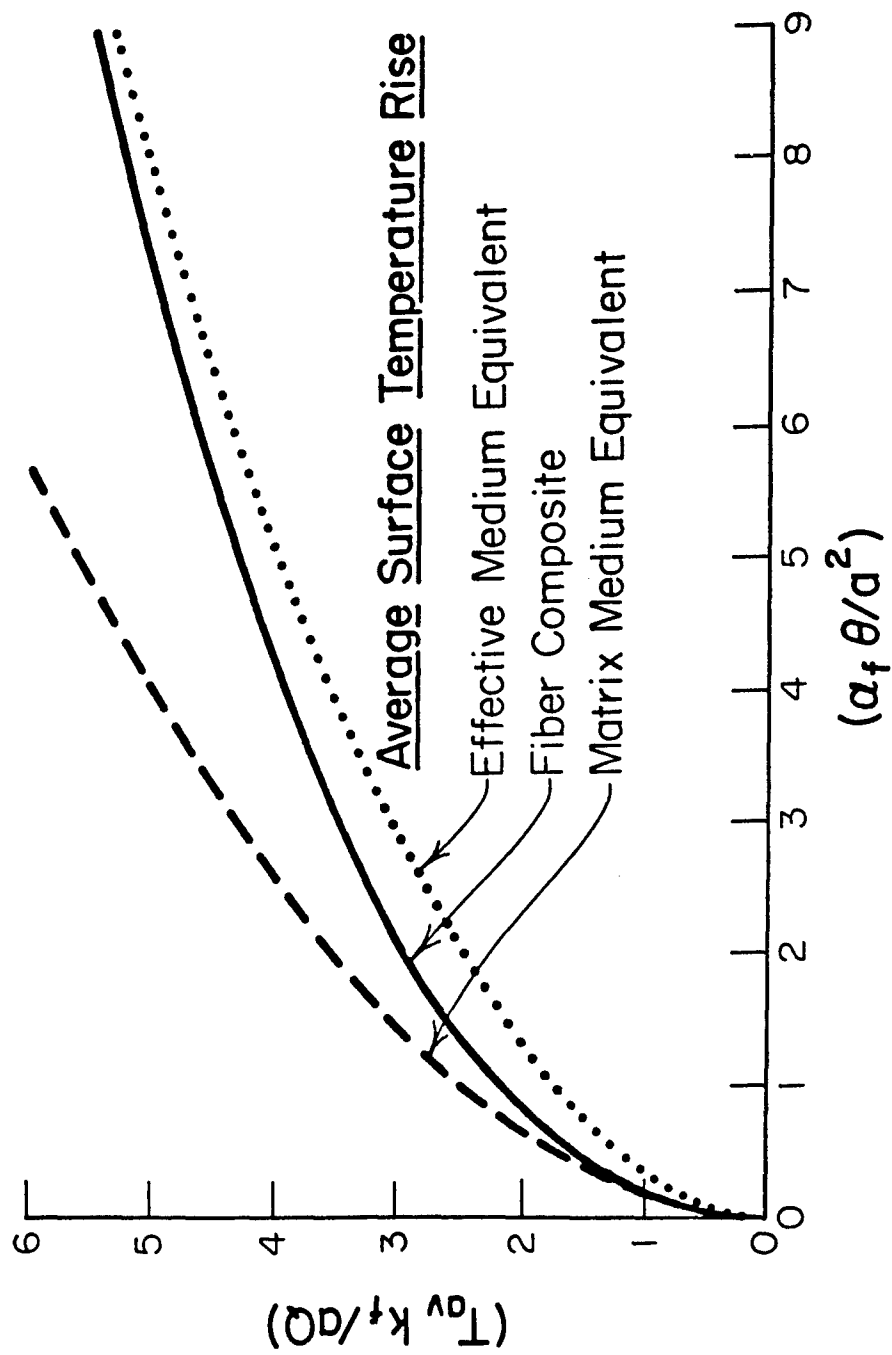


Figure 3.6. Average surface temperature rises, Case 6

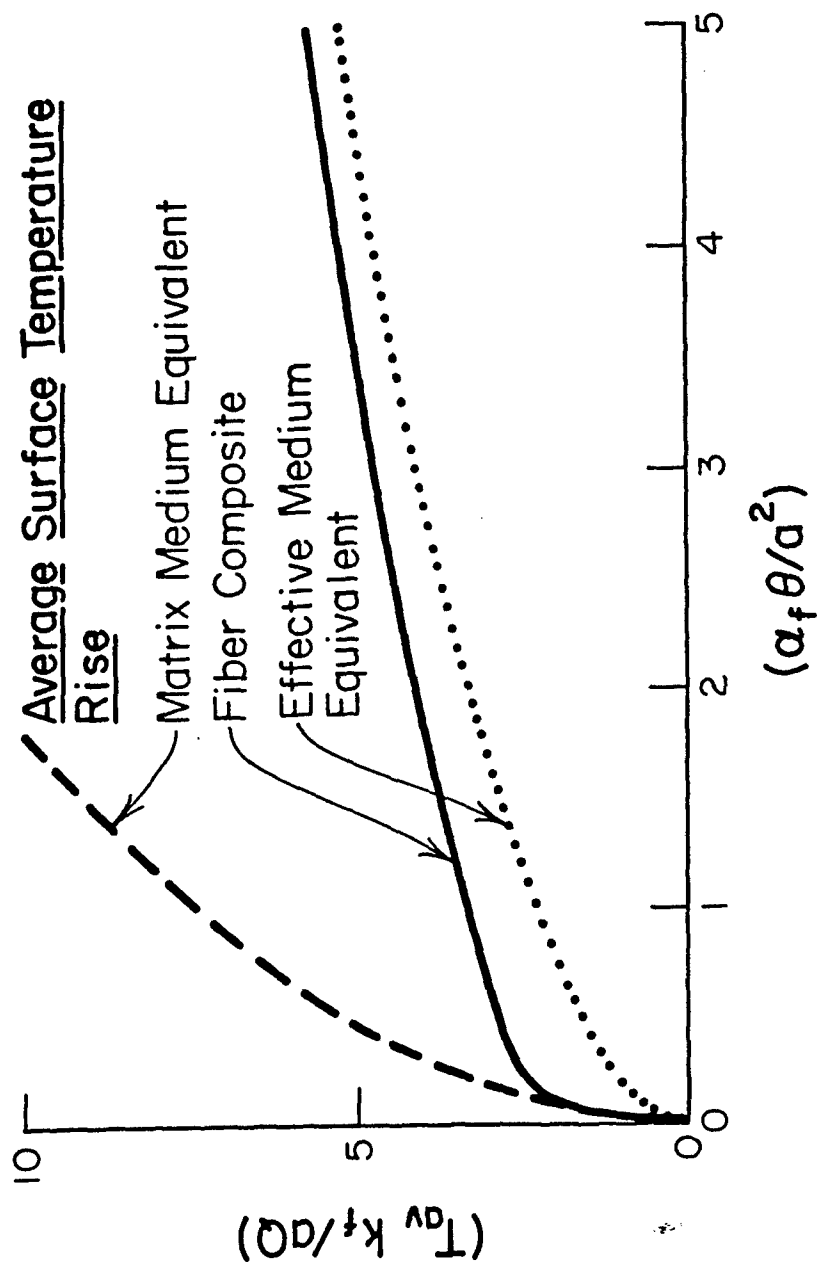


Figure 3.7. Average surface temperature rises, Case 7

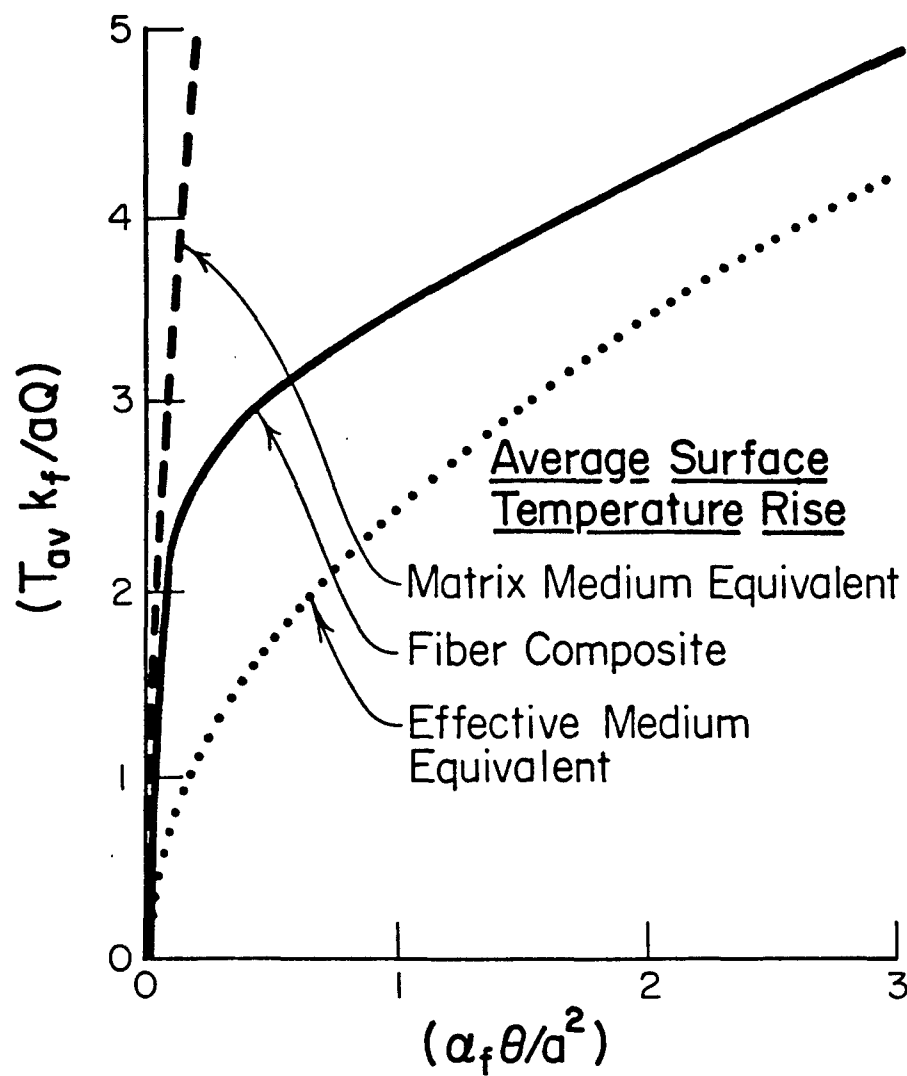


Figure 3.8. Average surface temperature rises, Case 8

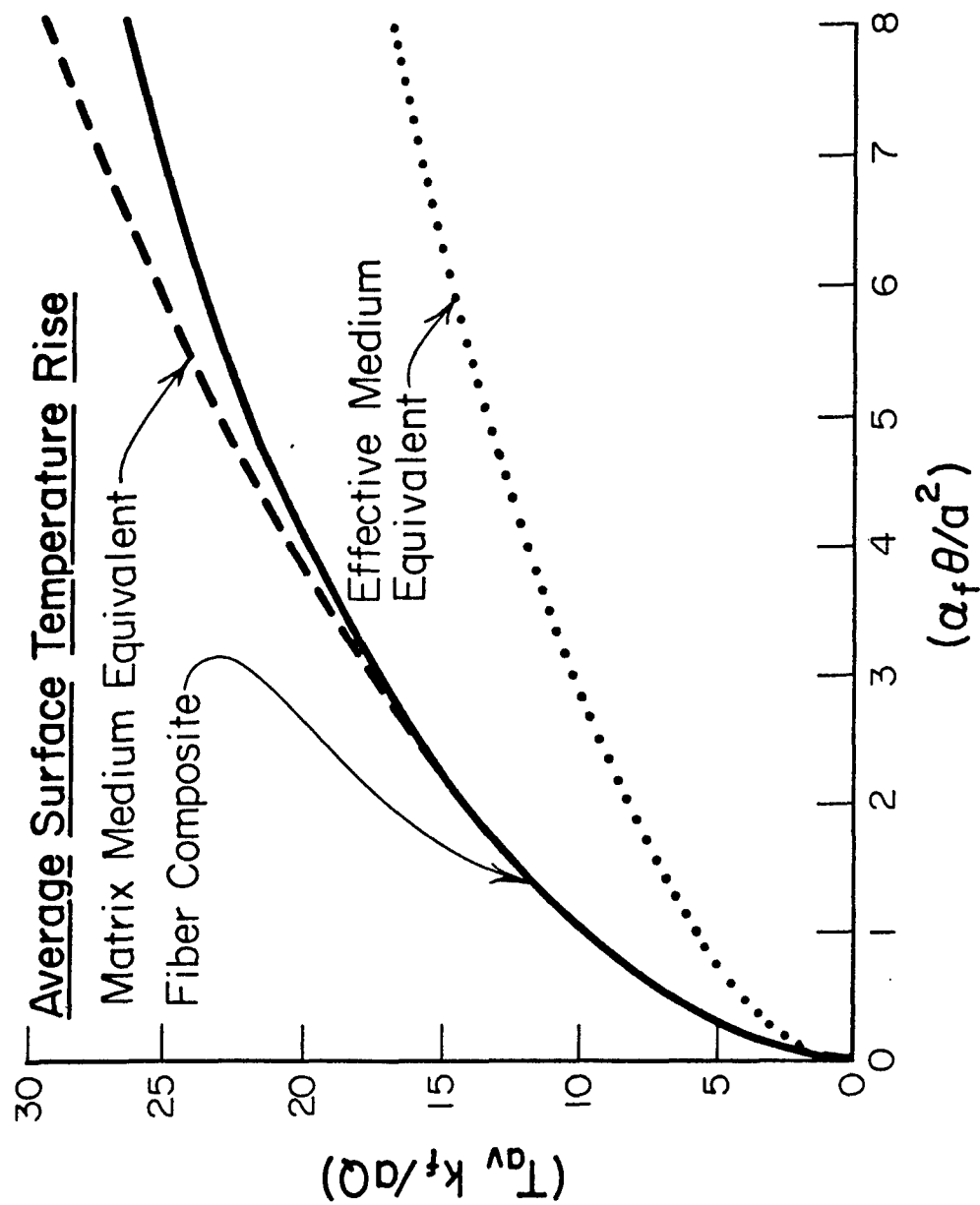


Figure 3.9. Average surface temperature rises, Case 9

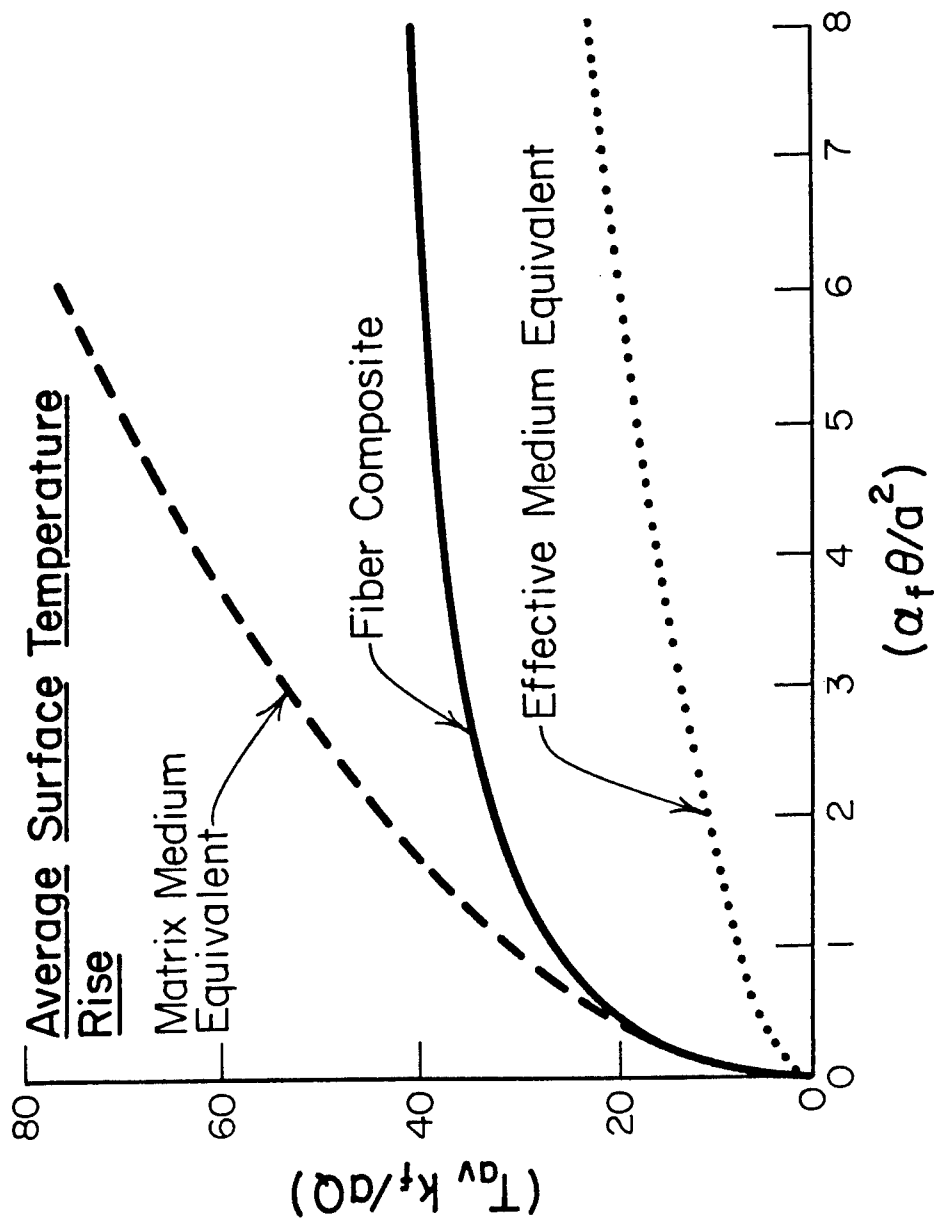


Figure 3.10. Average surface temperature rises, Case 11

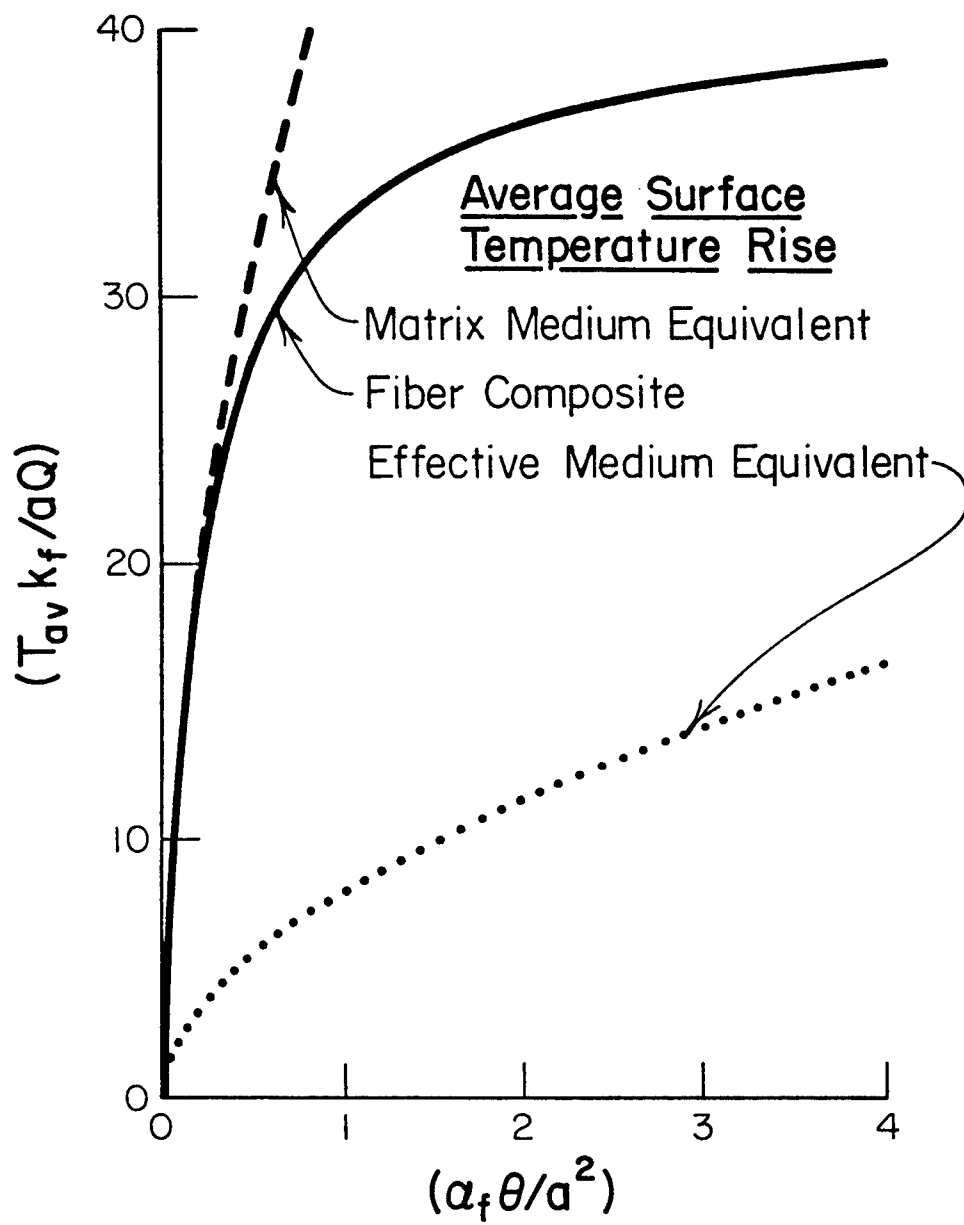


Figure 3.11. Average surface temperature rises, Case 12

and effective-bound temperature variations being close to one another; consequently, graphic representations of the composite surface temperature variations would not be revealing in confirming or refuting the concept of time threshold. Case 9 was not included, for the early-time threshold time of 41.6 requires excessive computer time in order to reach beyond the first limit; for Case 4, the fiber and the matrix properties are identical and no graph is needed.

Returning to the criteria of threshold-time demarcation, Figure 3.3 shows that the surface temperature variation of the composite whose properties are defined as Case 1 in Tables 3.2 and 3.3 is virtually described by the upper limiting bound (in this event, the effective bound) very near the later-time threshold of $\bar{\theta}_{t-2} = 5.9$; while at or near the early-time threshold $\bar{\theta}_{t-1} = 0.165$, the temperature variation is almost indistinguishable from the lower limiting bound (the matrix bound).

For the composite defined by Case 2, the average surface temperature variation with time is shown in Figure 3.4. While it is difficult to discern the behavior near the early-time threshold, it is quite definite that the surface temperature is identical to that of the upper limiting bound (the effective-bound). For the temperature variation shown in Figure 3.5 for Case 3, that calculated for the composite is nearly parallel but not identical to the upper (effective) bound, the upper time limit of $\bar{\theta} = 8$. This is because of the later-time threshold of $\bar{\theta}_{t-2} = 10$ for Case 3; whereas it is equal to 2 for Case 2.

The physical-property combination of Case 6 and those of the succeeding cases as well give the effective-bound as the upper limit. For Case 6, Table 3.2 gives values of 0.5 and 9.0 for the early-time and later-

time thresholds; it can be established quite clearly that the composite surface temperature shown in Figure 3.6 does follow these two limiting bound curves at the determined threshold time values. For Case 7 and Case 8, the upper and lower bounds of the temperature-time curves indicated in Figures 3.7 and 3.8 show greater discrepancies from each other than other cases; however, the trend of the calculated surface temperature variations - following at first the matrix bounds up to the early-time thresholds of 0.056 and 0.026, then deviating towards the effective bounds near the later-time thresholds of 5.0 and 4.8 - is quite apparent.

The temperature variation shown in Figure 3.9 for Case 10 gives a close scrutiny of the early-time behavior as the calculated value gradually deviates from the matrix-bound starting from $\bar{\theta} = 0$ to $\bar{\theta} = \bar{\theta}_{t-1}$ of 8.52 at which the calculated value is still much closer to the matrix-bound than to the effective-bound. As the later-time threshold is 102, the limited span of the calculations did not permit a close examination of the temperature-time curve at later times. For Case 11 and Case 12, shown in Figure 3.10 and 3.11, a further confirmation of the early-time threshold concept is found in that the matrix-bound temperatures are nearly identical to those computed for the composite surfaces. However, for both cases, the later-time thresholds are too large to permit an examination of the later-time events.

III.4 TRANSVERSE DISTRIBUTIONS OF THE COMPOSITE SURFACE TEMPERATURES

Unlike a one-medium temperature response, the surface temperatures of composites with uni-directional fibers are not found uniform across a repeating element, as defined in Figure 3.1, from $\bar{y} = 0$ to $\bar{y} = 1.25$.

During the very early stage of a heating process, i.e., for $\bar{\theta}$ much less than $\bar{\theta}_{t-1}$, the composite surface (and, in fact, the entire body) responds in an almost identical fashion to that of a half-space body consisting of the matrix material only.

As heating proceeds, crossing over the early-time threshold, the influence of the embedded fibers begins to assert itself and the resulting surface temperature distribution from $\bar{y} = 0$ to $\bar{y} = 1.25$ becomes more non-uniform. Near $\bar{y} = 0$, aligned with the fiber centers, the surface temperature rise deviates from the matrix-bound towards the effective-bound. These two bounding temperatures have been defined by Equations III.8 and III.9. At or near $\bar{y} = 1.25$, which is situated between rows of fiber centers, the surface temperature rise is less influenced by the presence of the fibers. Whether the surface temperature at $\bar{y} = 0$ is higher or lower than at $\bar{y} = 1.25$ depends on the relative magnitudes of the two temperature bounds, defined by Equations III.8 and III.9. Since the two surface temperature rises are inversely proportional to the physical-property combinations $\sqrt{k_e(\rho c)_e}$ and $\sqrt{k_m(\rho c)_m}$, the relative values for all twelve cases are tabulated in the last two columns of Table 3.2.

Between the limiting times of the early-time threshold $\bar{\theta}_{t-1}$ and later-time threshold $\bar{\theta}_{t-2}$, the level of the surface temperature undergoes transition from the matrix-bound trend towards the effective-bound trend. Also, the surface temperature variation from $\bar{y} = 0$ to $\bar{y} = 1.25$ exhibits a maximum degree of non-uniformity in this period of transition time. The variation can be, therefore, described as follows: The local temperature at $\bar{y} = 0$ has its value corresponding, crudely speaking, to the effective-

bound temperature; the surface temperature varies towards $\bar{y} = 1.25$ where it approaches the matrix-bound level. In the interior of the composite body, conduction in the y-direction smears the sharp temperature profile existing on the surface of the composite.

Upon further heating, resulting in a time scale exceeding the later-time threshold $\bar{\theta}_{t-2}$, surface temperature non-uniformities tend to diminish, as the entire body becomes more like a single medium characterized by the effective thermal properties.

The sequence of events which compartmentalize the surface temperature variations with time in the different time periods of a heating process is of crucial importance in evaluating responses of all fibrous composites undergoing any diffusion-controlled process, for example, heat flow transient or moisture infiltration. To illustrate these events more specifically and to ascertain the validity of the criteria established for these events, two non-dimensional times $\bar{\theta} = 1$ and $\bar{\theta} = 8$ were selected and the surface temperature variations in the transverse direction from $\bar{y} = 0$ to $\bar{y} = 1.25$ were computed for the twelve cases in this numerical study. A more demonstrative combination of the physical properties is afforded by those prescribed by Case 7 characterized by the following:

- (i) early-time threshold, $\bar{\theta}_{t-1} = 0.06$
- (ii) later-time threshold, $\bar{\theta}_{t-2} = 5.0$
- (iii) matrix-bound temperature rise factor
 $1 / \sqrt{k_m(\rho c)_m} = 6.16 \times 10^{-2}$
- (iv) effective-bound temperature rise factor
 $1 / \sqrt{k_e(\rho c)_e} = 1.95 \times 10^{-2}$

For this case, the matrix medium, if alone by itself, would have a temper-

ature rise three times as large as that of the effective-medium equivalent. The time scale of $\bar{\theta} = 1$ is substantially larger than the early-time threshold, $\bar{\theta}_{t-1}$, but is still much less than the later-time threshold, $\bar{\theta}_{t-2}$. At a larger time of $\bar{\theta} = 8$, the later-time threshold is well exceeded. For these two time instants, the computed surface temperature variations are indicated in Figure 3.12.

Apparent to inspection is the observation that when the time scale is $\bar{\theta} = 1$ between the two thresholds, the non-uniformity from $\bar{y} = 0$ to $\bar{y} = 1.25$ is quite appreciable; the variation is from 2.8 to 3.9 with a transverse average value of 3.4. This accounts for a 30 percent excursion of the mean value. At the same time instant, the effective-bound temperature rise (applicable near $\bar{y} = 0$) is 2.34 and the matrix-bound rise (applicable near $\bar{y} = 1.25$) is 7.55. With an early-time threshold $\bar{\theta}_{t-1} = 0.06$, the temperature-time history of the surface is well within the transition period.

At a larger time of $\bar{\theta} = 8$, the surface temperature distribution becomes more uniform; it varies from a value of $\bar{T} = 6.6$, near $\bar{y} = 0$, to a value of $\bar{T} = 7.6$, near $\bar{y} = 1.25$, resulting in a mean value of 7.14. The variation is 15 percent of the mean. At this larger time of $\bar{\theta} = 8$, which is well over the later-time threshold of $\bar{\theta}_{t-2} = 5.0$, the effective-bound value is 6.75 and the matrix-bound value becomes 21.4; the computed transverse-average surface temperature of 7.14 indicates its asymptotic approach toward the effective-medium prediction. Relevant to the preceding discussion is the time variation of the transverse-average surface temperature presented in Figure 3.7 for Case 7, where close proximity of the composite surface temperature and the effective-bound prediction is striking.

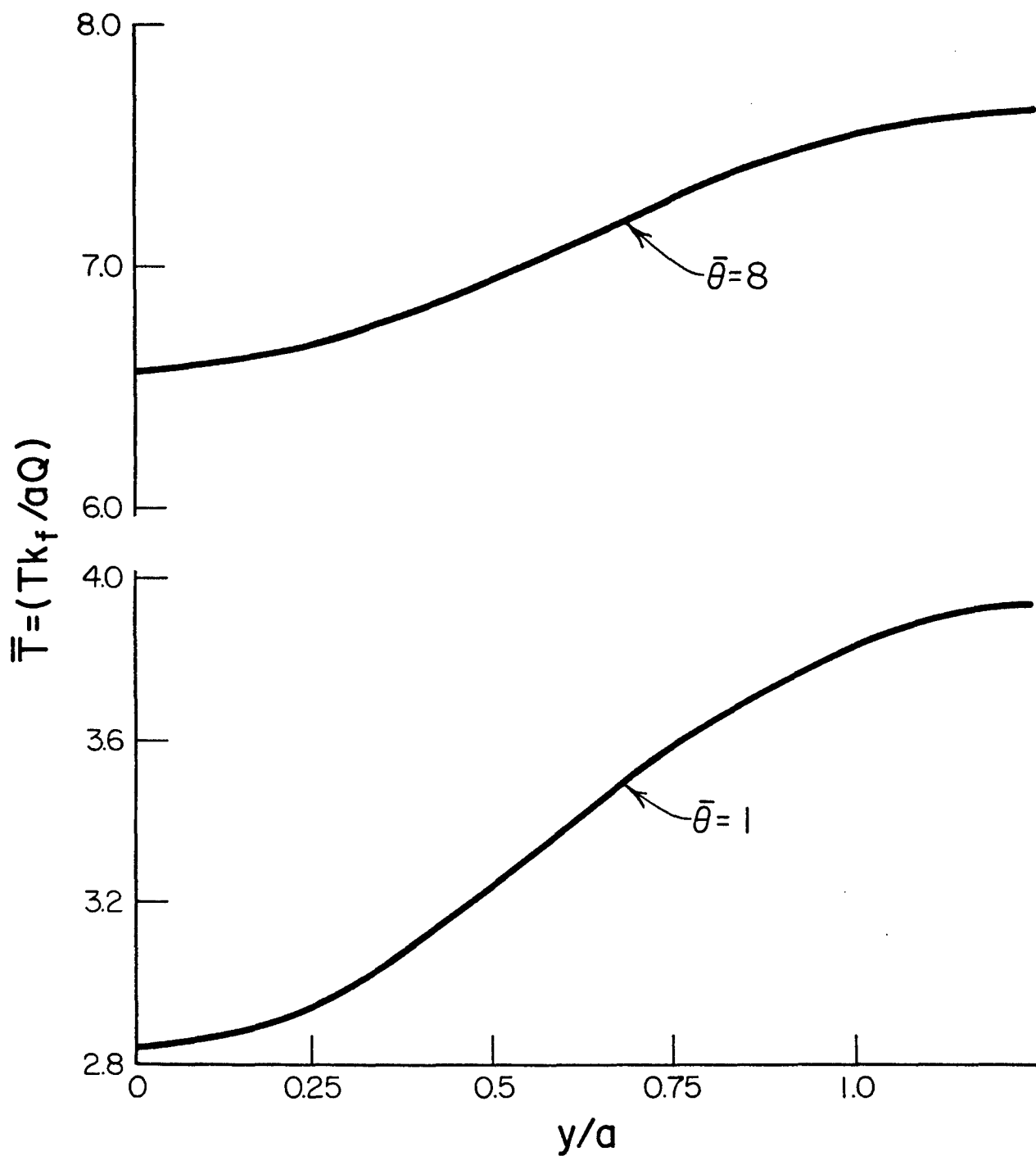


Figure 3.12. Transverse variations of the surface temperatures at $\bar{\theta} = 1$, Case 7

III.5 TEMPERATURE DISTRIBUTIONS ALONG THE HEAT-FLOW DIRECTION

A more demanding evaluation of the proposed criteria is the interior temperature distributions of a composite body in comparison with the asymptotic temperature distributions of the effective-bound on the one hand and of the matrix-bound on the other. The closeness of an actual temperature distribution with either one of the two bounds is governed by the two time thresholds. First, transverse-average temperatures in the interior of a composite is considered. It is defined by erecting a cross-section perpendicular to the x-axis of Figure 3.1 and the average cross-sectional temperature is obtained by weighting with the thermal inertias of the materials such a cross-section contains. Thus, there results:

$$\bar{T}_{av} = \frac{\int_f (\rho c)_f \bar{T}_f d\bar{y} + \int_m (\rho c)_m \bar{T}_m d\bar{y}}{f(\rho c)_f + m(\rho c)_m} \quad (III.10)$$

where the symbols, f and m , now denote the extents of the fiber and matrix regions along the cross-section. When used as subscripts, the meaning is obvious. Equation (III.10) defined the transverse-average temperature, in compliance with the energy conservation concept.

For highlighting the interior temperature variations with reference to the asymptotic solution bounds, the twelve cases of physical-property combinations were first examined with regard to their potential for demonstration. Cases 3, 4, 5 and 6 were ruled out, because the limiting bounds given by Equations III.8 and III.9 were too close to each to give meaning-

ful comparisons. Cases 9 through 12 were not used because their later-time threshold values were too large which would require excess computing time for creditable comparisons. Of the remaining cases, 7 and 8 are nearly alike and so are 1 and 2. Hence, Case 1 and Case 7 are used for demonstrating the validity of the asymptotic temperature solutions.

Case 1 Temperature Responses. Tables 3.1 and 3.2 list the characteristic values for the physical-property combination. The surface temperature rise based on an effective-medium is 1.66 times as large as the matrix-bound value. The early-time and later-time thresholds are 0.17 and 5.9, respectively. And in order to span over these two time limits, the transverse-average temperature variations along the principal heat flow direction x are calculated at time intervals of $\bar{\theta} = 0.1, 0.25, 0.50, 4$ and 10 .

At $\bar{\theta} = 0.1$, the computed transverse-average temperature profile is shown in Figure 3.13. Since the early-time threshold is $\bar{\theta}_{t-1} = 0.17$, the computed average temperature profile is compared with the profile based on the matrix-bound equivalent; the latter is also shown in Figure 3.13. Some discrepancy between these two distribution curves is noted. If the effective-bound curve was used, the departure of the composite average temperature profile would be much greater, since the latter is 1.66 times the matrix-bound reference curve.

For a larger time value, $\bar{\theta} = 0.25$, the average temperature profile and the matrix-bound temperature distribution shown in Figure 3.14 show a greater discrepancy from each other than in Figure 3.13. Further on, as the time is increased to $\bar{\theta} = 0.5$, the computed composite temperature-profile is compared with the effective-medium limit, as is done in Figure 3.15

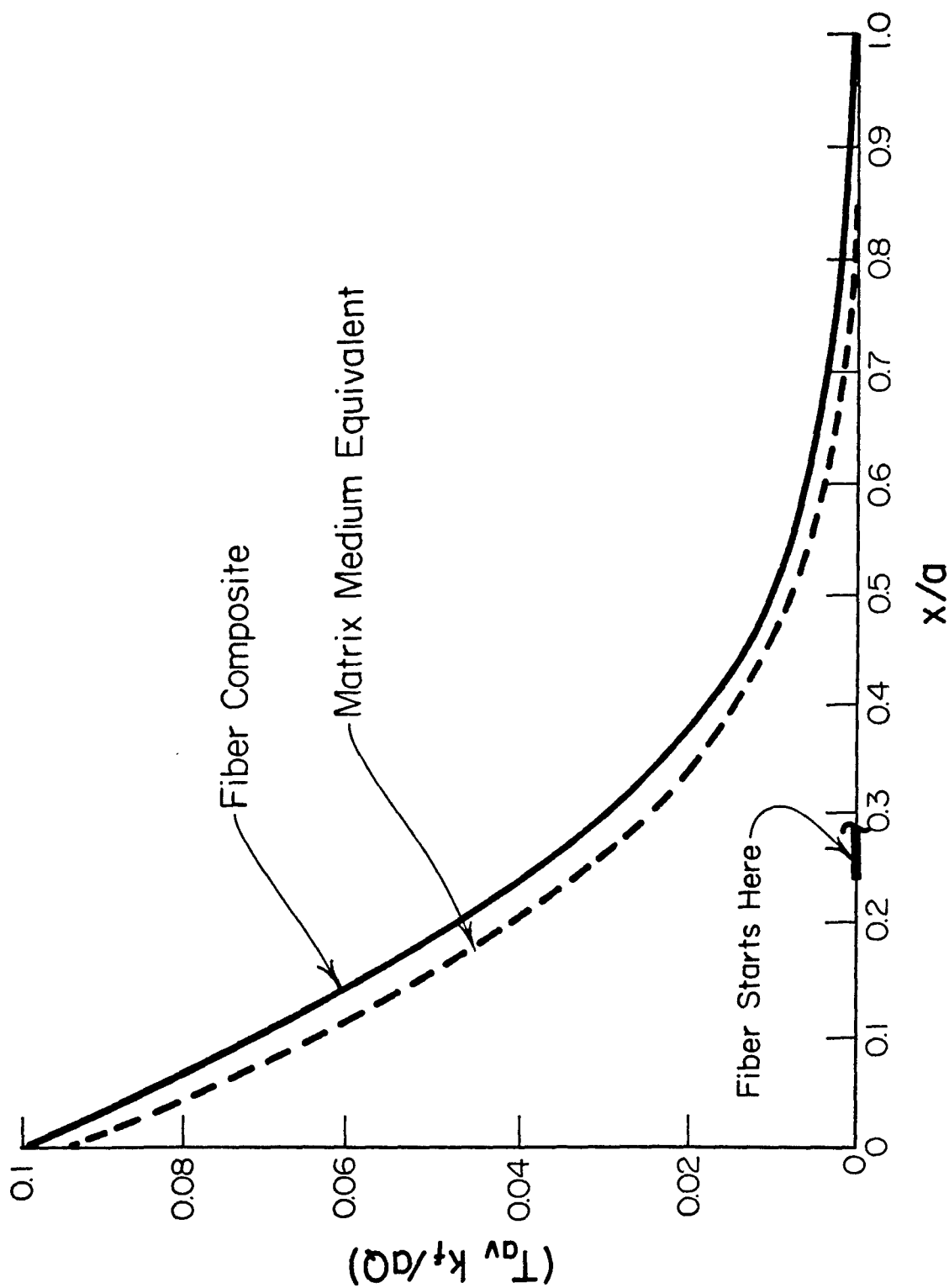


Figure 3.13. Transverse-average temperature profile in the x -direction at $\bar{\theta} = 0.1$, Case 1

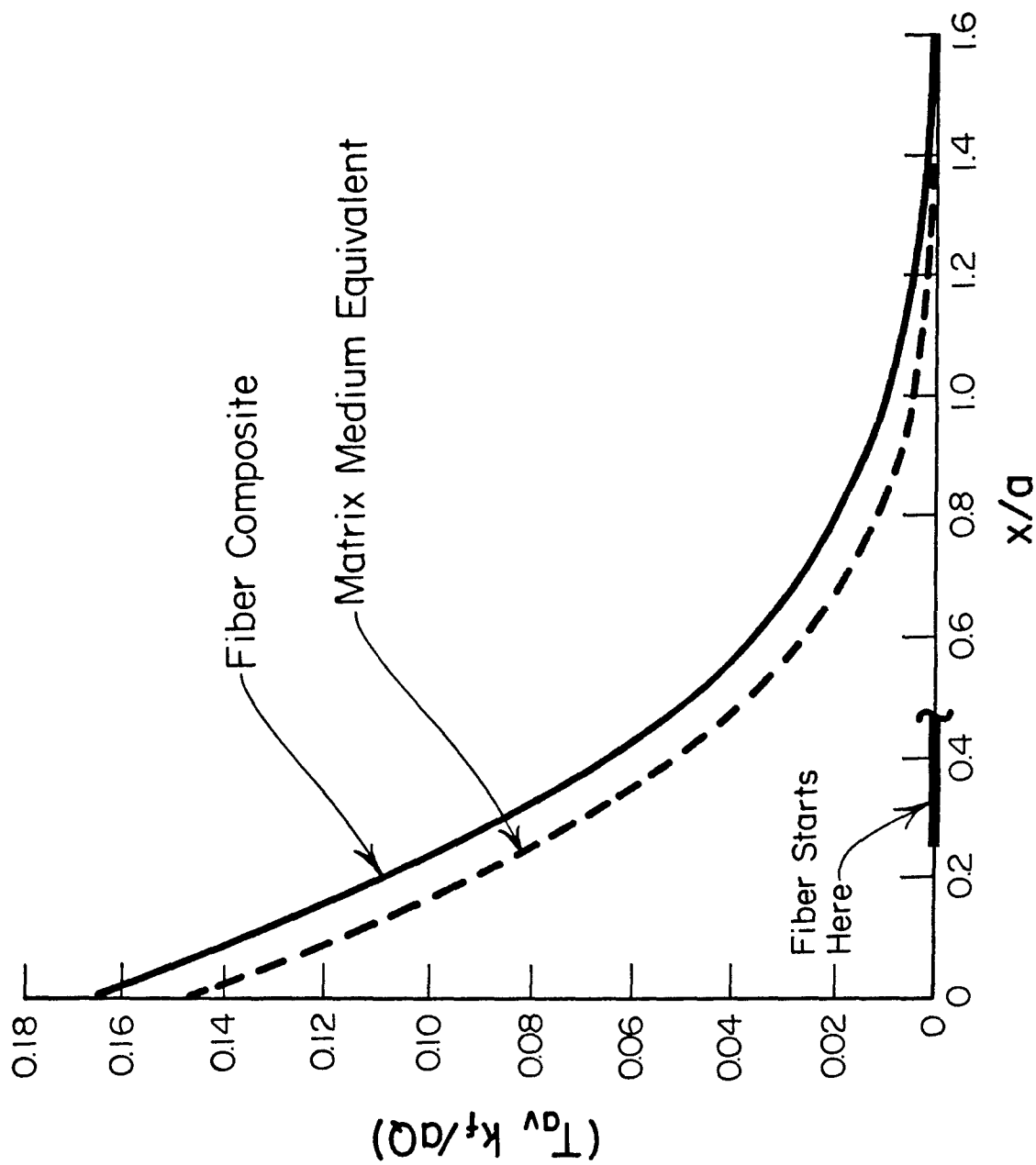


Figure 3.14. Transverse-average temperature profile in the x-direction at $\bar{\theta} = 0.25$, Case 1

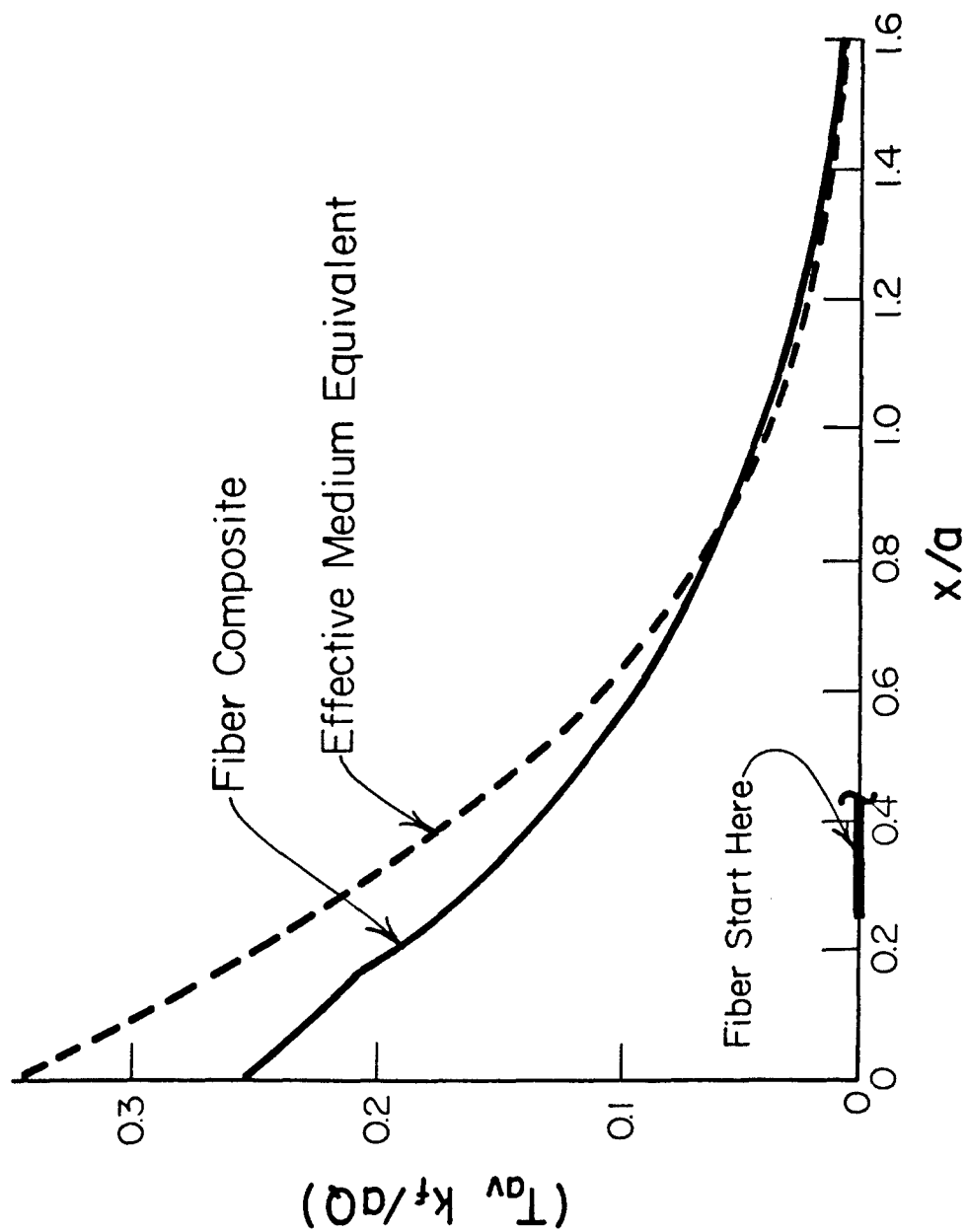


Figure 3.15. Transverse-average temperature profile in the x-direction at $\bar{\theta} = 0.50$, Case 1

and in succeeding illustrations for $\bar{\theta} = 4$ and 10. For $\bar{\theta} = 0.5$, the composite temperature response is in a transition stage and the temperature variation shown in Figure 3.15 indicates substantial departure from the effective-medium limit as well as from the matrix-medium limit (not shown in Figure 3.15). At still larger values of time $\bar{\theta} = 4$ and 10, for which the computed temperature profiles are displayed in Figures 3.16 and 3.17, the composite transverse-average temperature profiles are nearly the same as that of the effective-medium calculations. It is of significance to note that the temperature comparison shown in Figure 3.16 for $\bar{\theta} = 4$ indicates a very minute temperature rise at $\bar{x} = 5$. In other words, the finite configuration of Figure 3.1 in which only two fibers were included is virtually equivalent to a semi-infinite configuration with more fibers after the second one. For the time instant defined in Figure 3.16, i.e., $\bar{\theta} = 4.0$, the effective-medium prediction is therefore the same as the solution for a semi-infinite medium given by Equations III.2 and III.3 in which the subscript m is replaced by the subscript e. For $\bar{\theta} = 10$, at which time the temperature distributions are contained in Figure 3.17, the effective-medium limit is that of a finite region response, i.e., the insulated boundary condition at $\bar{x} = 5$ is taken into account. In both figures for $\bar{\theta} = 4$ and 10, the local influence of the fibers in affecting the average temperature distribution is noted in slope discontinuities. For the combination of the physical properties of Case 1, the fibers are assumed less conductive than the matrix material, i.e., $k_f/k_m = 0.34$; this ratio results in a steeper slope of the heat path across the fiber than across the matrix material only. (For Case 7, the ratio of the conductivities is reversed, as shall be discussed later.)

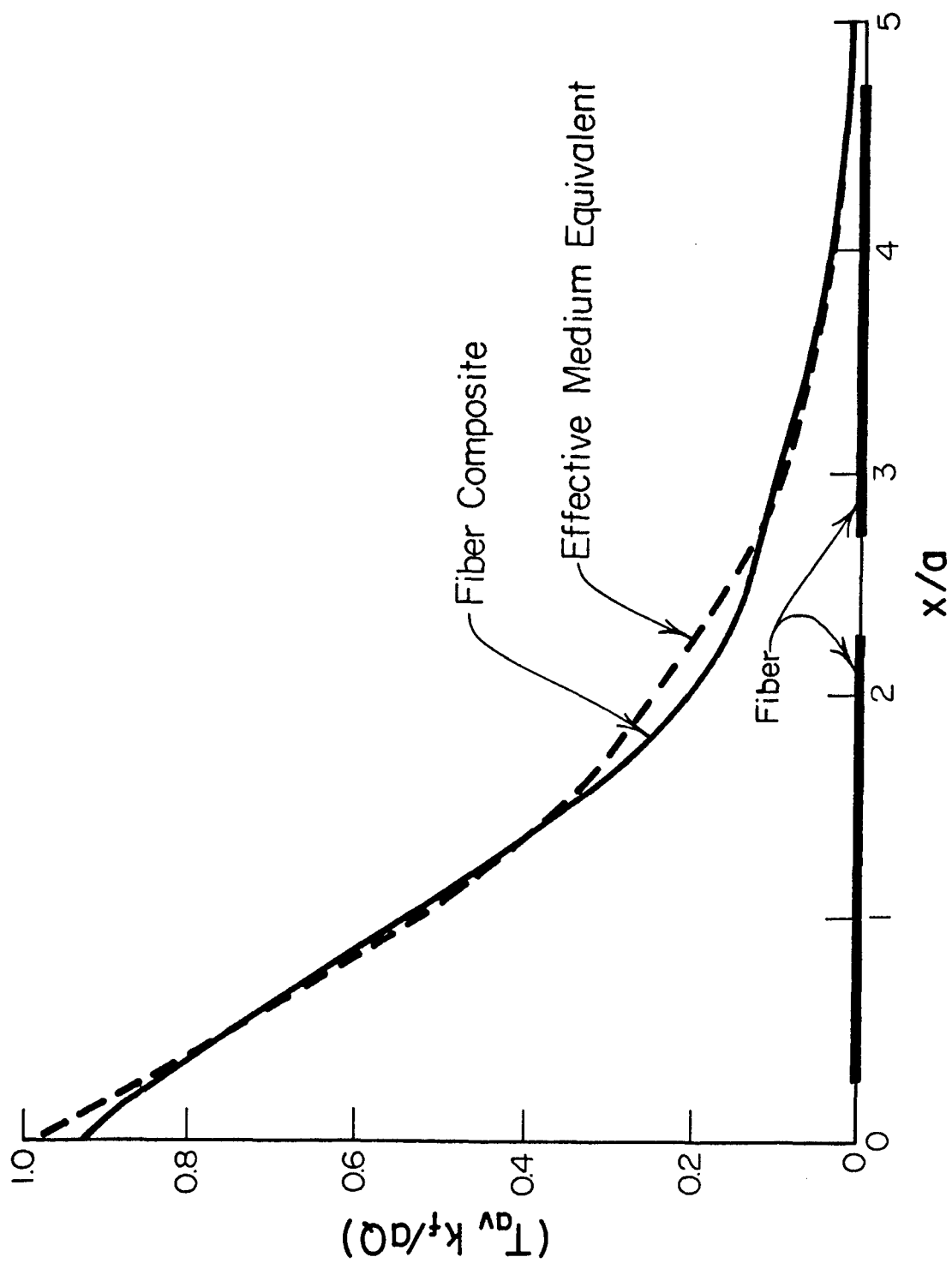


Figure 3.16. Transverse-average temperature profile in the x-direction at $\bar{\theta} = 4$, Case 1

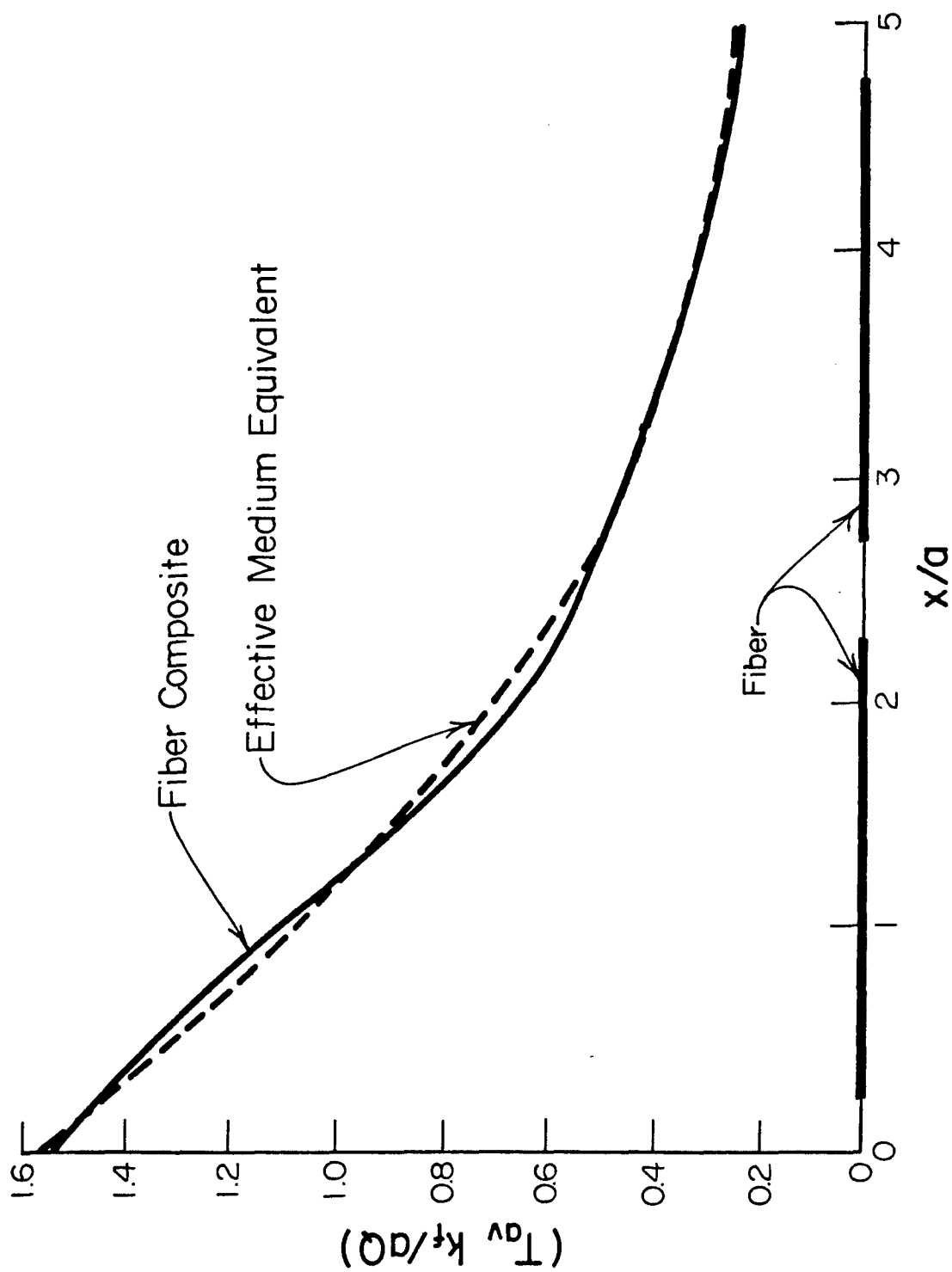


Figure 3.17. Transverse-average temperature profile in the x -direction at $\bar{\theta} = 10$, Case 1

To probe further into the usefulness of the threshold criteria, two-dimensionality of the temperature distributions in the composite interior are examined. In Figure 3.18 are shown the temperature profiles along the x -direction at selected values of y . The distributions shown are valid for $\bar{\theta} = 0.5$, which is more than the early-time threshold but is much less than the later-time threshold value. At a fixed x -position, the temperature variances at different transverse stations can be readily identified. They are more pronounced near the surface than in the interior. The interfacial positions characterized by a slope discontinuity are marked by a circle-symbol. At a larger time $\bar{\theta} = 5$ which is almost equal to the later-time threshold, the corresponding temperature profiles are displayed in Figure 3.19, in which transverse variances occur only near the surface $x = 0$ but are much less pronounced. These distributions at different transverse positions are nearly identical to each other and are amply represented by a single effective-medium curve which for simplicity's sake is omitted from Figure 3.19.

Preceding discussions based on the calculated temperature responses of a two-fiber composite give sufficient credence and support to the threshold time criteria in establishing the temperature bounds by demonstration with the Case-1 physical property combination. The later-time threshold can be stated another way which is perhaps more useful: By the time the heat front has, based on the calculation using an effective-medium replacement, reached the lee-side of the first fiber encountered in the heat path, a one-dimensional effective-medium is henceforth a satisfactory replacement model for the temperature response in a real composite, except with respect to the local variance of the fibers.

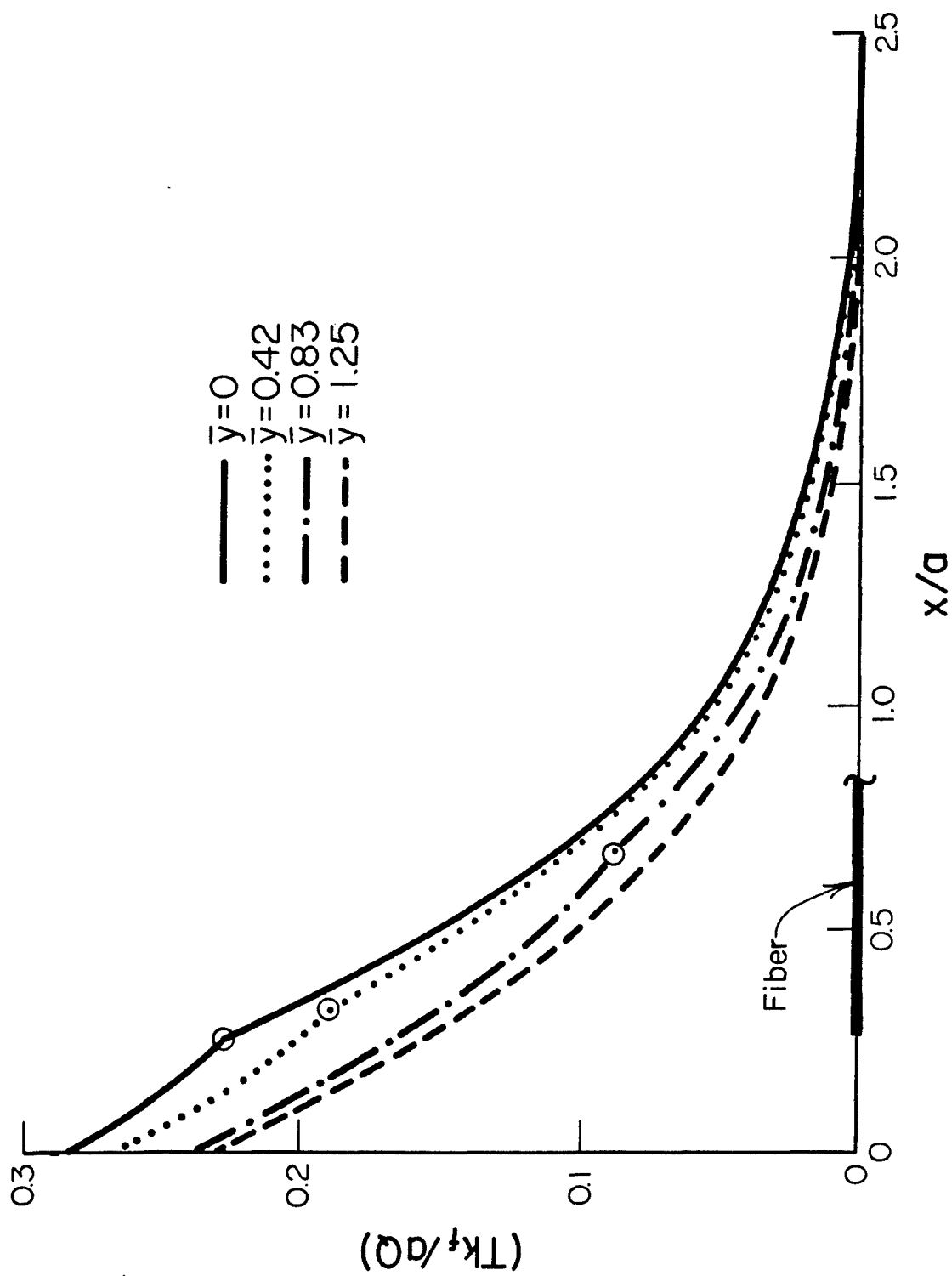


Figure 3.18. Two-dimensional temperature distribution in composite, $\bar{\theta} = 0.5$, Case 1

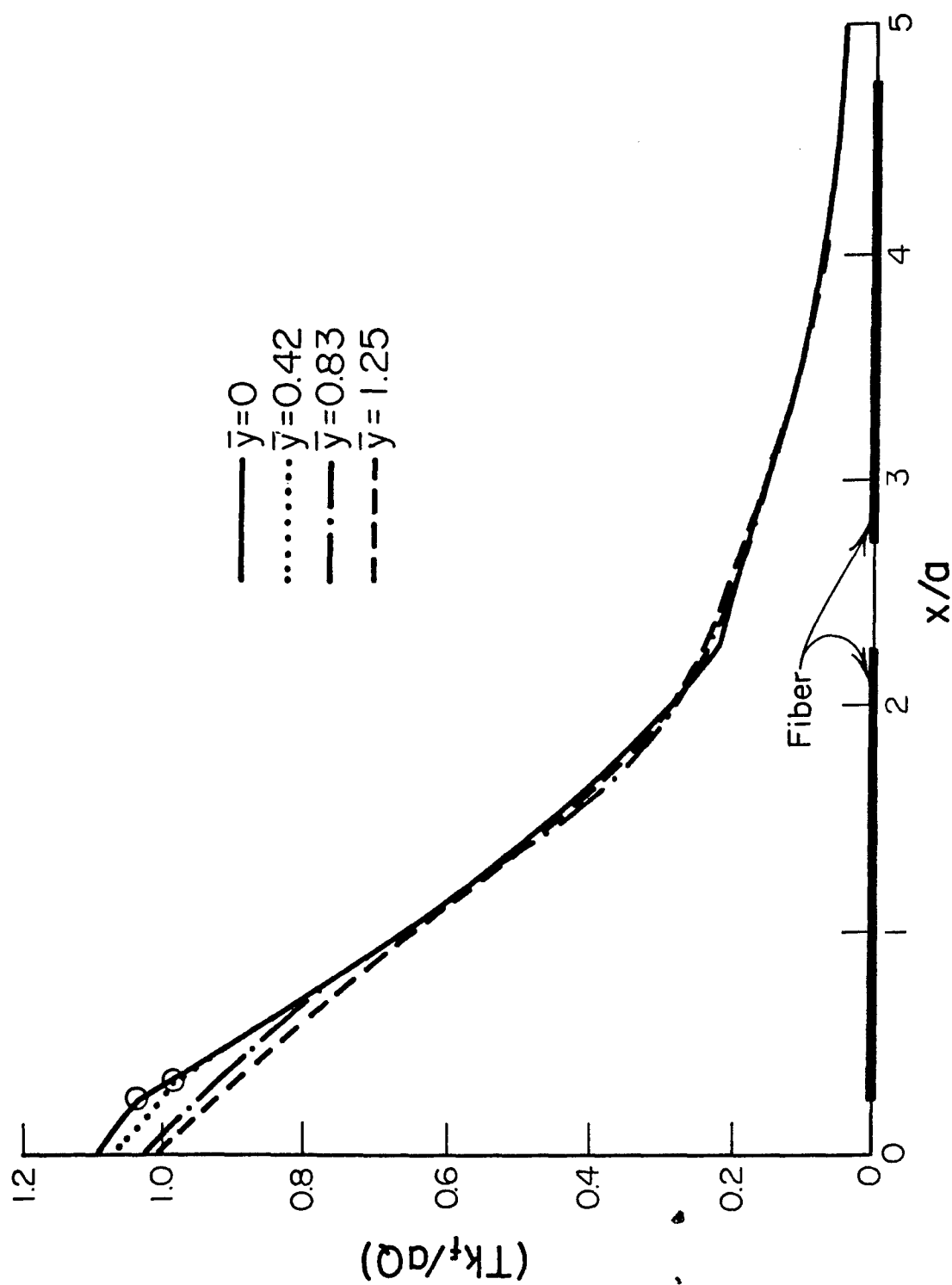


Figure 3.19. Two-dimensional temperature distribution in composite, $\bar{\theta} = 5.0$, Case 1

Case 7 Temperature Responses. The physical properties of the constituents for this combination are such that there is an appreciable difference between the two limiting reference temperatures - the matrix-bound and the effective-bound. The former is three times as large as the latter. Another distinguishing feature is the large fiber/matrix conductivity ratio of 5.0 for this particular combination.

To evaluate the thermal responses for this case, the transverse-average temperature variations with the depth direction are presented first in Figures 3.20 and 3.21 at time instants of $\bar{\theta} = 0.5$ and $\bar{\theta} = 5$, respectively. In conjunction with the times selected, it should be mentioned that the threshold times are 0.06 and 5.0, as given in Table 3.2. Thus the first time instant selected is over the early-time threshold but is short of the later-time threshold value. It is therefore expected that the averaged temperature distribution along the depth direction will be neither the effective-bound nor the matrix-bound. The curves shown in Figure 3.20 attest to this observation, particularly near the surface location. On the surface ($x = 0$), the composite average temperature rise is about 2.9 while the effective-bound gives a value of 1.7 and the matrix-bound yields a temperature of 5.4. This means that the average composite surface temperature has migrated toward the effective-bound through an appreciable range, beginning from the matrix-bound level.

At a later time of $\bar{\theta} = 5$, however, the effect of the conductivity disparity begins to appear even though the overall agreement between the composite transverse-average temperature and the profile on the basis of an effective medium appears good. Figure 3.21 illustrates this observation. The distinct slope changes at $\bar{x} = 0.3$, 2.2 and 2.7, although having

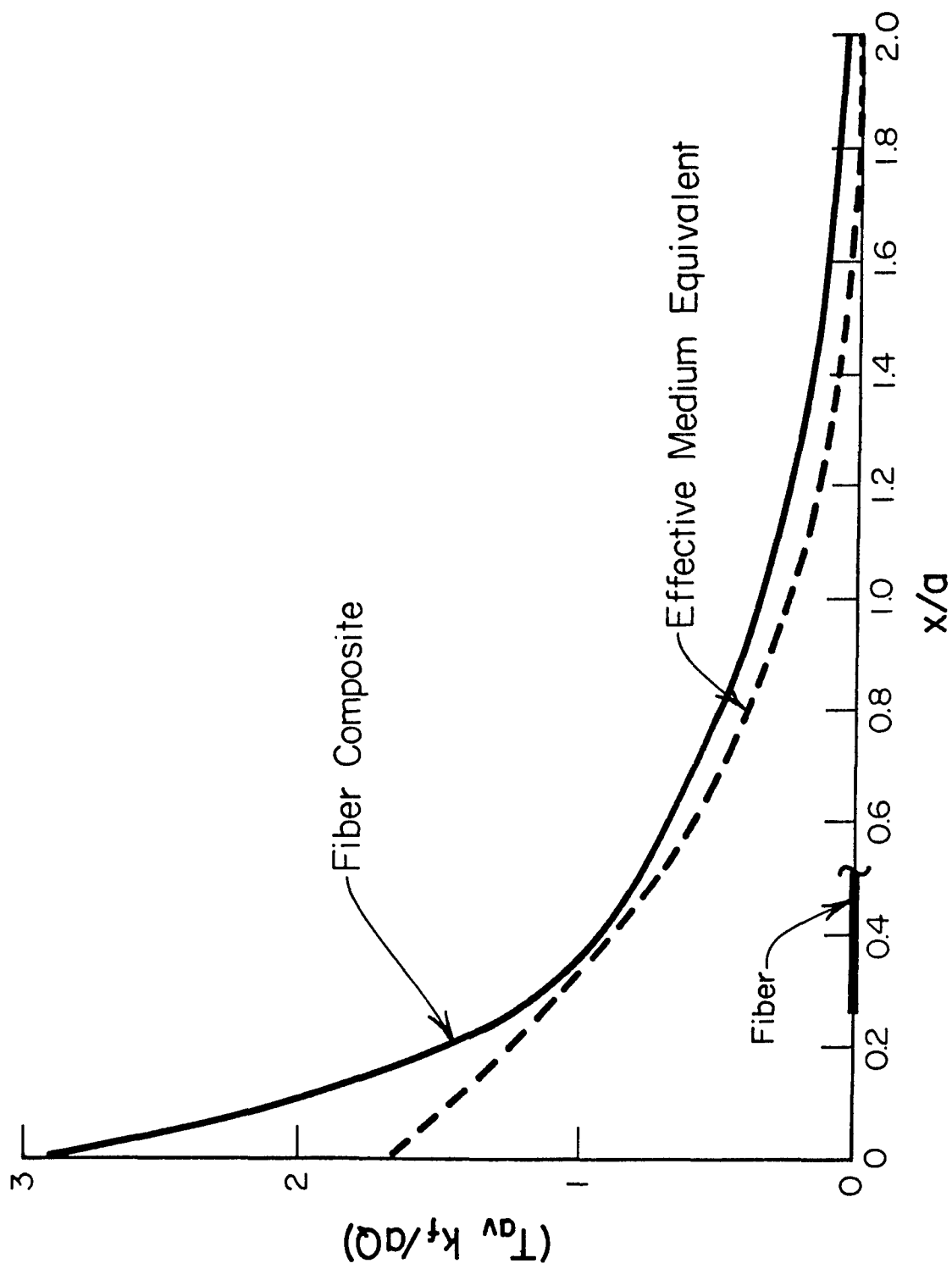


Figure 3.20. Transverse-average temperature profile in the x -direction at $\bar{\theta} = 0.5$, Case 7

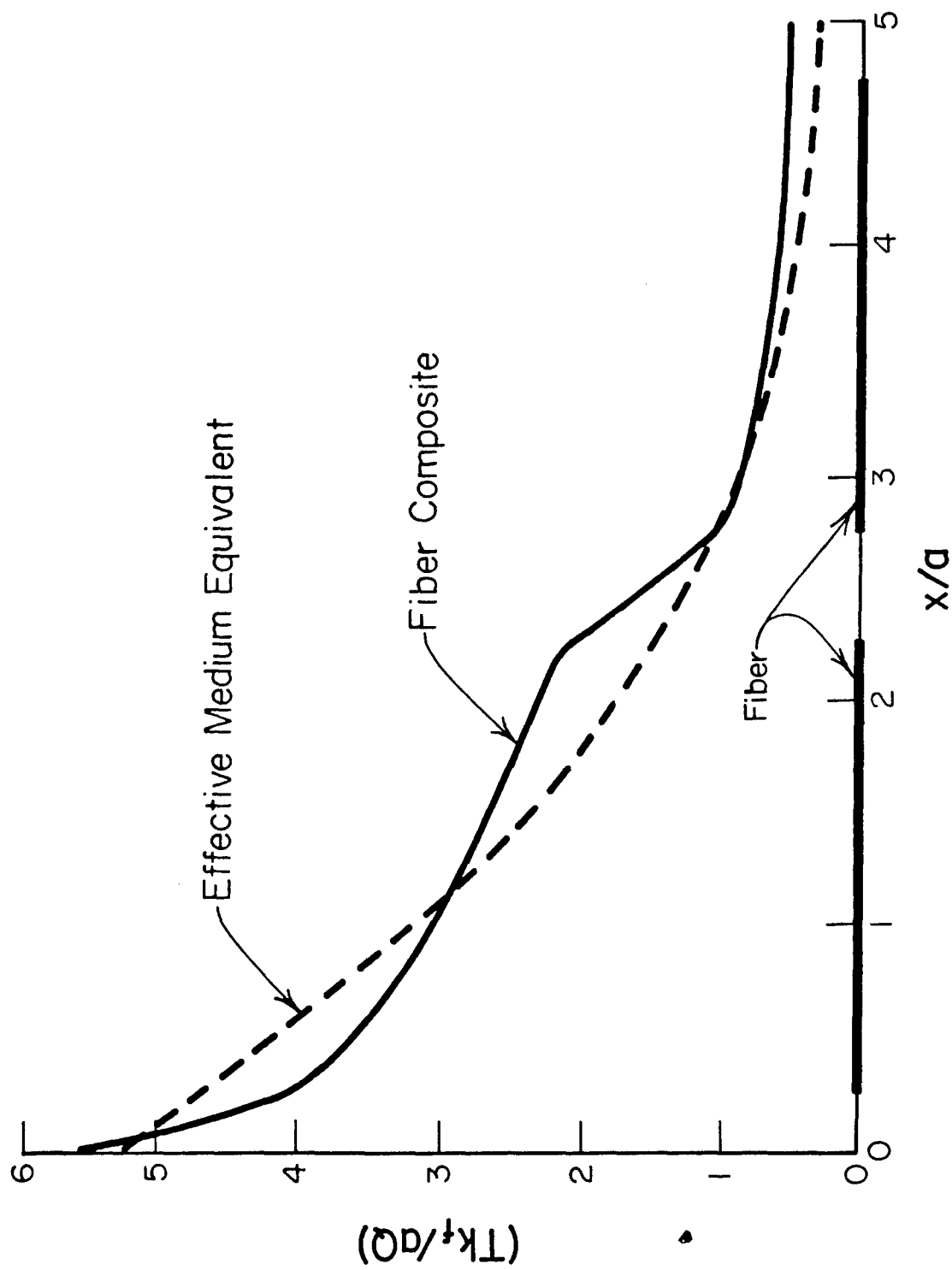


Figure 3.21. Transverse-average temperature profile in the x-direction at $\bar{\theta} = 0.5$, Case 7

been averaged at these positions, demonstrate the conductivity-ratio effect very markedly.

Further demonstration of the conductivity-ratio influence is found in the temperature distribution patterns in the interior of the composite configuration. Shown in Figures 3.22 and 3.23 are the two-dimensional patterns of the temperature responses for $\bar{\theta} = 0.5$ and $\bar{\theta} = 5.0$, respectively. In both illustrations, there is very little transverse temperature variation (at different y-positions), except near the heating surface. A larger transverse variation is noted on the surface for the time scale of $\bar{\theta} = 0.5$ than for $\bar{\theta} = 5.0$, and discontinuities in the temperature gradient (located by the circle symbols) are more visually prominent than those displayed in the temperature patterns for Case 1. It must be mentioned that for Case 1, the ratio of the conductivities, k_f/k_m , is 0.34, while for Case 7, the ratio becomes 5, i.e., k_m is more than k_f in the Case 1 combination and their relative values are reversed. For Case 7, the temperature gradient is larger in the matrix region; and for Case 7, the gradient is less. Visually speaking, the influence of the temperature-gradient appears more pronounced in Case 7 than in Case 1; in reality the influence in both cases is numerically equal but in different directions.

The transverse-average temperature variation with time for the cross-section of $\bar{x} = 1.25$, where the first fiber center is located, is shown in Figure 3.24 together with that predicted based on the effective-medium equivalent; closeness between these two variations with time especially after $\bar{\theta} = 5$ is an additional confirmation of the time-threshold concept advanced in Section III.2.

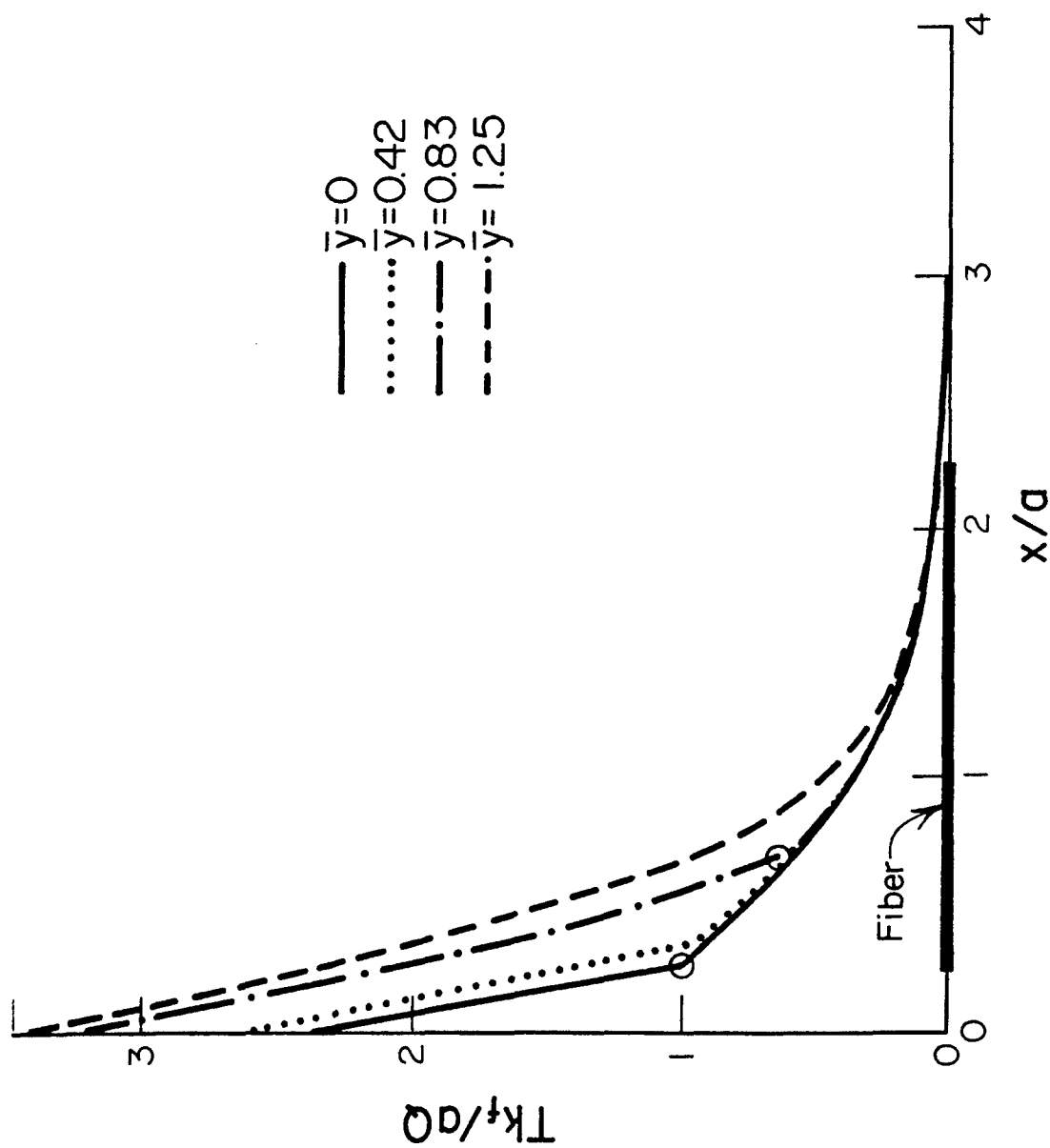


Figure 3.22. Two-dimensional temperature distribution in composite, $\bar{\theta} = 0.5$, Case 7

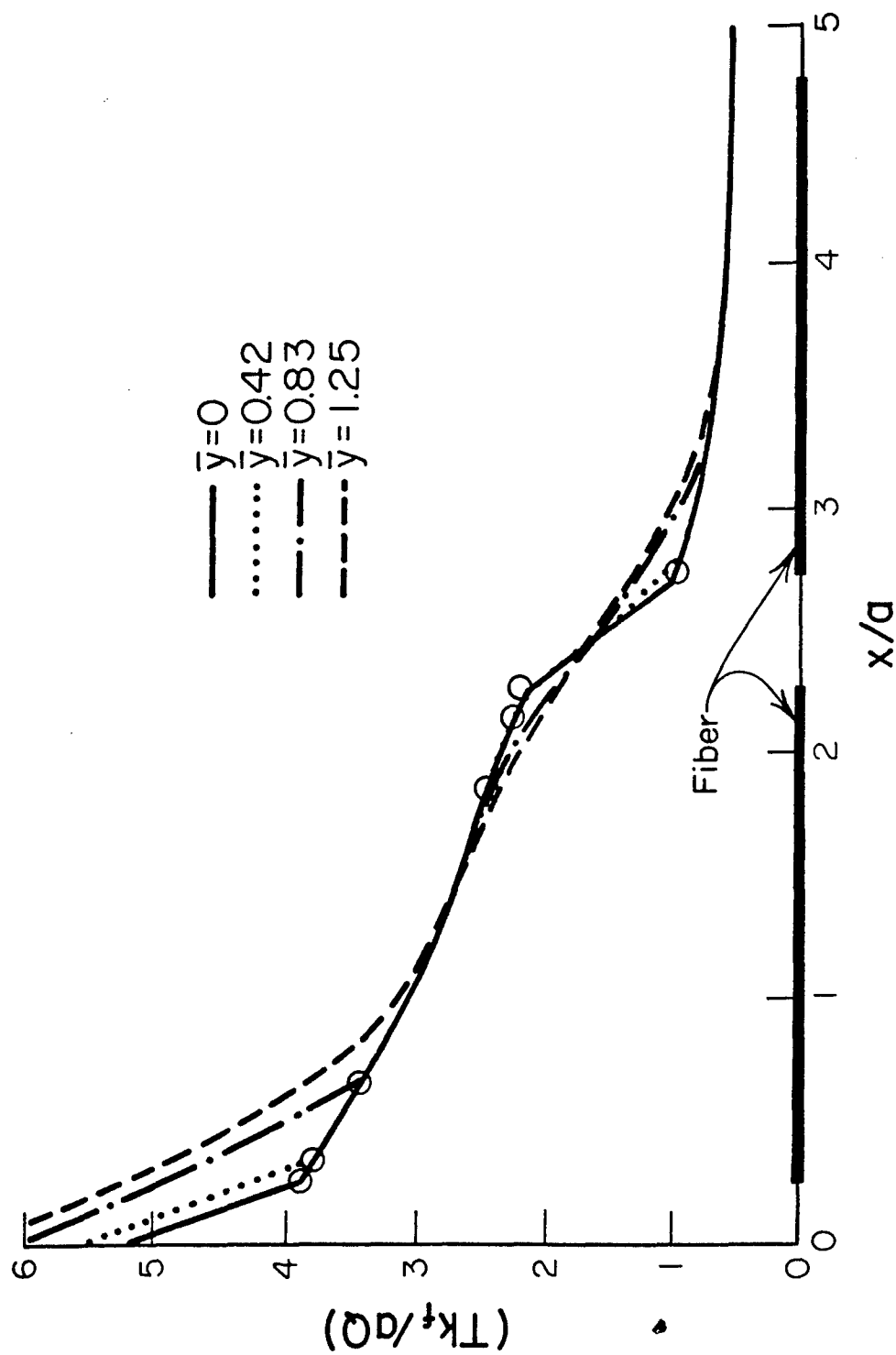


Figure 3.23. Two-dimensional temperature distribution in composite, $\bar{\theta} = 5.0$, Case 7

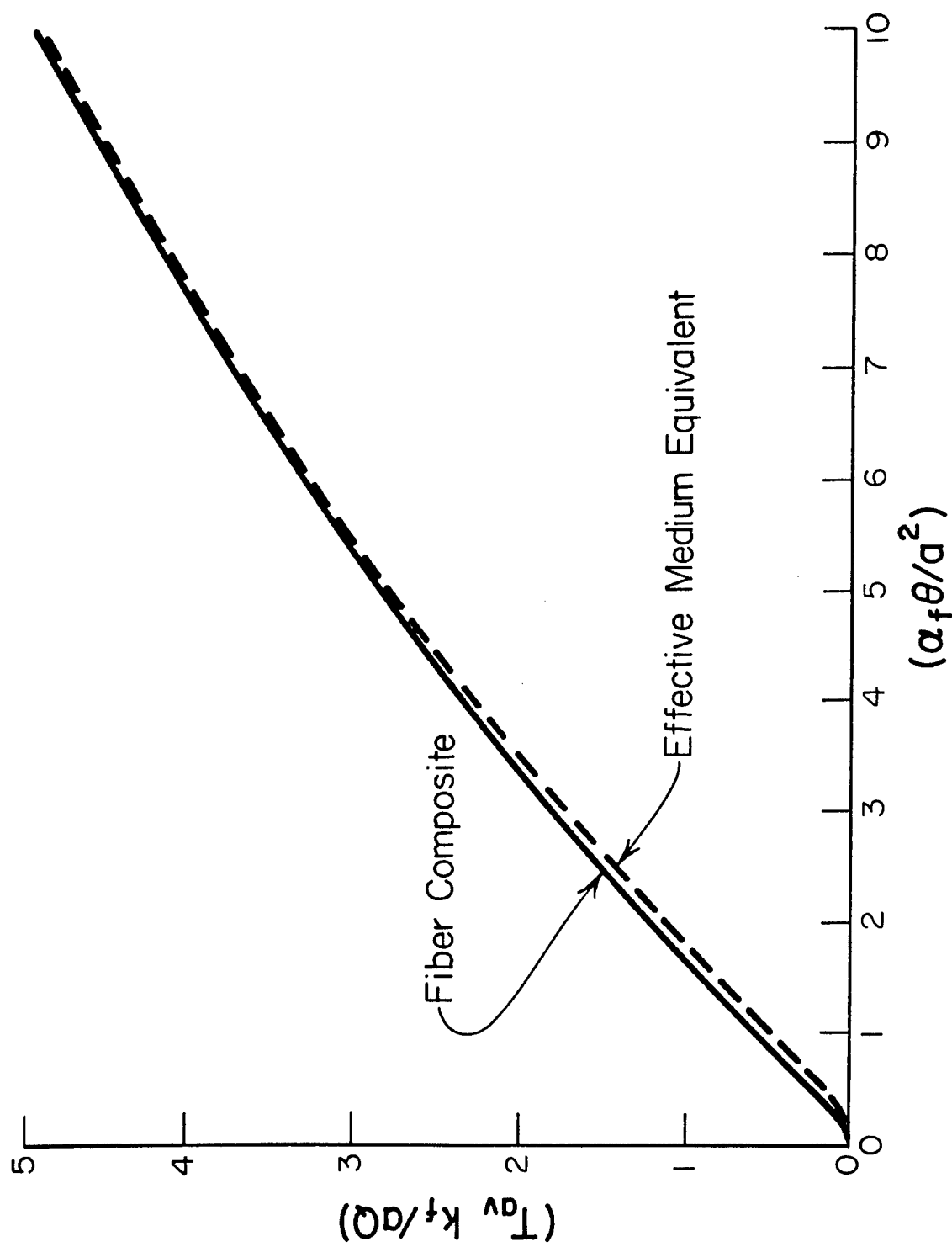


Figure 3.24. Transverse-average temperature rise at $\bar{x} = 1.25$, Case 7

SECTION IV

CONCLUSION

Unsteady-state heat conduction in fibrous composite materials when the heat flow direction is transverse to uni-directional fibers has been considered in this report. Because of the complex nature of physical and geometrical parameters involved in the problem, an analytical solution, if not impossible, is a mean task. Thus, a numerical approach was made by using an explicit finite-difference method to approximate the solutions to governing partial differential equations.

The fiber and matrix thermal properties, as well as the volume ratio, are the determining factors in the temperature response of the fibrous composite materials. These composites appear with a variety of volume ratios in industries. Considering these wide varieties, it is impossible to analyze the temperature responses for all volume ratios with different thermal properties for the fiber and matrix materials. Thus, only a typical value of 0.5 was considered. The choice of this value for the volume ratio is deliberate; it resembles the same volumes for the fiber and matrix materials and can be used as a good reference for analyzing temperature responses of composites with lower or higher volume ratios.

In total, twelve cases were considered. These twelve cases are arrived at by first varying the ratio of (k_e/k_m) from 0.6 to 3.0 with intermediate values of 1.0 and 2.0. Next, the ratios of the thermal capaci-

ties $(\rho c)_e/(\rho c)_m$ are varied from 0.6 to 1.0 with intermediate steps of 1 and 5. From these desired values and in combination with the rule of mixtures, i.e.,

$$(\rho c)_e = v_f(\rho c)_f + v_m(\rho c)_m$$

the values of $(\rho c)_m$ can be determined as a part of the original specifications. The thermal conductivity k_m to be specified is fixed by the desired ratio (k_e/k_m) and the information in Reference [2] which relates the ratios (k_f/k_m) and (k_e/k_m) .

The temperature responses of these twelve cases when a uniform heat flux is imparted on their surfaces were analyzed to determine the influences of the parametric combinations, i.e., the thermal conductivity and thermal capacity ratios. The influences of these parameters which are the most important factors from a heat conduction viewpoint are discussed extensively in Section III of this report.

The criteria of dividing a heating process into an early-time threshold and a later-time threshold appear quite valid and useful in estimating the temperature responses of composite materials. For heating times less than the early-time threshold, the surface temperature of a composite body containing uni-directional fibers, when heat flow occurs across the fiber axis, is asymptotically governed by a half-body occupied by the matrix material only. And for heating times greater than the later-time threshold, the effective-medium predicts the composite temperature responses quite well. Inbetween these two thresholds, considerable temperature variation occurs in the transverse direction as well as between the fibers and the immediate matrix material surrounding the fiber.

The later-time threshold can be more conveniently expressed as the time required for heat flux to penetrate through a layer of one-fiber dimension deep below the heating surface.

REFERENCES

- [1] Han, L.S., Transient Heat Flow Along Uni-Directional Fibers in Composites, AFWAL TR-82-3061.
- [2] Han, L.S. and Cosner, A.A., Conduction Heat Transfer Analysis in Composite Materials, AFWAL-TR-80-3012.